Effect of steps and surface coverage on rates and kinetic isotope effects for reactions catalyzed by metallic surfaces: Chemisorption of hydrogen on Ni

ARTICLE *in* THE JOURNAL OF PHYSICAL CHEMISTRY · OCTOBER 1990

Impact Factor: 2.78 · DOI: 10.1021/j100384a052

2 AUTHORS:

Thanh Truong
University of Utah
168 PUBLICATIONS **6,156** CITATIONS
SEE PROFILE

Donald Truhlar
University of Minnesota Twin Cities
1,342 PUBLICATIONS **79,615** CITATIONS
SEE PROFILE

Effect of Steps and Surface Coverage on Rates and Kinetic Isotope Effects for Reactions Catalyzed by Metallic Surfaces: Chemisorption of Hydrogen on Ni

Thanh N. Truong and Donald G. Truhlar*

Department of Chemistry and Supercomputer Institute, University of Minnesota, Minneapolis, Minnesota 55455-0431 *(Received: January 30, 1990)*

We present a new parametrization for the embedded-diatomics-in-molecules (EDIM) potential energy function that is significantly more accurate than the previous one for the interactions of two H atoms with a Ni surface or with a third H atom. Thus, it can be used to study lateral interactions of H_2 with H, and it is also parametrized for a system of three H atoms on a Ni surface. In addition, the metal atom parameters are independent of which layer the metal atom is in so there is no ambiguity in studying reactions at steps or kinks. We apply canonical variational transition state theory with semiclassical transmission coefficients to investigate the dynamics of the dissociative chemisorption of gas-phase H_2 molecules on both single-crystal-face and stepped Ni(100) surfaces. We also consider the effect of additional H atoms, and we compre results for clean and partially covered surfaces. We find that classical transition-state recrossing and quantal tunneling effects are very important in the dissociation of H_2 on the clean Ni(100) surface. The presence of a step on the metal surface is found to increase the rate of chemisorption significantly, while somewhat decreasing the kinetic isotope effect (KIE). Conversely, the presence of adsorbed H atoms is found to decrease (poison) the chemisorption rate, although it increases the KIE. The results are consistent with experimental observations. Finally, the exchange reaction on Ni(100) is found to proceed most favorably by a two-step mechanism consisting of dissociative chemisorption of H_2 followed by recombination with a coadsorbed H atom.

1. Introduction

In a previous paper,[1] we have presented a new semiempirical formalism, called embedded diatomics in molecules (EDIM), for the energies of molecules interacting with metal surfaces. The parameters were adjusted so that binding energies, dissociative chemisorption barriers, surface diffusion barriers, and vibrational frequencies for H and H_2 on the three low-index faces of Ni are all in reasonably good agreement with experiment. The resulting potential energy function is possibly the most accurate potential function currently available for two H atoms interacting with any metal, and it provides the opportunity for detailed dynamical studies. In the present study, we consider some technologically important applications of this energy function, namely, we explore the question of enhanced (or poisoned) chemical reactivity due to surface imperfections such as steps, the possibility of surface catalyzed exchange reactions on metallic surfaces, and the effect of surface coverage on dissociative chemisorption rates. We also consider the effect of steps and surface coverage on kinetic isotope effects (KIEs), which are an important diagnostic of mechanism. Although the present applications involve only two or three H atoms, we believe that they demonstrate the potential of the method. In addition the results are of intrinsic interest since the H_n/Ni system is a well-studied experimental system widely considered to be one of the best prototype cases for testing new theoretical approaches in surface science.

In order to improve the reliability of the method for treating reactions at steps and in the presence of ternary adatom interactions, we have now modified the parametrization presented previously. In section 2, we briefly summarize the EDIM formalism, and we discuss the new parametrization of the EDIM potential energy function. For dynamical calculations of reaction rates, we have applied canonical variational transition state theory (VTST) with semiclassical transmission coefficients, and the methods for these calculations are summarized in section 3. The results of the new parametrization for the topology of the potential energy function for one and two H atoms interacting with the three low-index faces of Ni are presented in section 4. Dynamical results for H_2 dissociative chemisorption on clean terraces or steps or on partially covered terraces on the (100) face of Ni are given in section 5. Finally, the possibility of hydrogen-exchange reactions on the Ni(100) surface is addressed in section 6.

(1) Truong, T. N.; Truhlar, D. G.; Garrett, B. C. *J. Phys. Chem.* **1989**, *93*, 8227.

2. Parametrization of the EDIM Potential Energy Function

2.1. Theoretical Formalism. EDIM theory is presented in full in the previous study,[1] so we present here only a brief summary.

For a system of N_g nonmetal atoms interacting with a metal surface that is represented by N_m metal atoms, the total potential energy V is separated into two contributions: V_M, which represents the metal–metal interactions within the solid, and V_{DIM}, which accounts for interactions between gas atoms and the metal and among the gas atoms. Thus

$$V = V_{DIM}[\{E_{kl}(\mathbf{x})\}_{k,l\neq k}^{N_g}, \{E_{kM}(\mathbf{x})\}_{k=1}^{N_g}] + V_M(\mathbf{x}) + E_0 \quad (1)$$

where the constant E_0 is the zero of energy which is chosen for convenience, and $\mathbf{x}$ is the collection of all atomic coordinate vectors and is given by

$$\mathbf{x} = \{\vec{r}_i\}_{i=1}^{N} \quad (2)$$

where N is the total number of atoms in the system, $N = N_g + N_m$, and $\vec{r}_i$ is a single atomic coordinate. For the present study, the coordinates of all metal atoms are fixed at their lattice geometries. For convenience in what follows, the indices are ordered such that $i = 1, ..., N_g$ are indices for the gas atoms, and $i = N_g + 1, ..., N$ are indices for the metal atoms.

The metal–metal potential, V_M, is given in EDIM by the embedded-atom method (EAM):[2]

$$V_M = \sum_{i=N_g+1}^{N} F_i[\rho_i(\mathbf{x})] + \sum_{i=N_g+1}^{N}\sum_{j>i}^{N} \phi_{ij}(R_{ij}) \quad (3)$$

where ϕ_{ij} is a pair potential depending on the distance R_{ij} between atoms i and j. Since all metal atom coordinates are fixed in the present study, we need not consider the second sum of (3) further. The first sum in (3), however, depends on all atomic coordinates. In this sum, ρ_i is the electron density at the location of atom i contributed by all other atoms (metal and nonmetal) in the system, and it is approximated as a sum over atomic densities, ρ_j^a, at the given point in space:

$$\rho_i = \sum_{j\neq i}^{N} \rho_j^a(R_{ij}) \quad (4)$$

The embedding function F_i in (3) is the attractive component of the energy of embedding atom i into a homogeneous electron gas of density $\rho_i(s)$; it is an empirical function for a given type of atom.[2]

(2) Daw, M. S.; Baskes, M. I. *Phys. Rev. Lett.* **1983**, *50*, 1285.

0022-3654/90/2094-8262$02.50/0

The first term, V_{DIM}, in (1) is given by diatomics-in-molecules (DIM) theory[3] in terms of the diatomic potential curves, E_{kl}, for the relevant electronic states of nonmetal atoms k and l and the pseudopotentials E_{kM} for the interactions between nonmetal atom and the surface. In the present study, we only consider interactions of effective one-electron nonmetal atoms with each other and with the metal surface, and as before,[1] we include only covalent configurations in the valence bond treatment. Consequently, the DIM potential is expressed in terms of singlet and triplet curves, E^1_{kl} and E^3_{kl}, for pairs k and l of nonmetal atoms, and in terms of analogous "singlet" and "triplet" pseudopotentials, E^1_{kM} and E^3_{kM}, respectively.

The singlet and triplet nonmetal–nonmetal interactions are modeled by Morse and anti-Morse potentials:

$$E^1_{kl} = D_{kl}\{1 - e^{-\alpha_{kl}(R_{kl}+R^{eq}_{kl})}\}^2 - D_{kl} \quad (5)$$

$$E^3_{kl} = \frac{1}{2}\left(\frac{1-\Delta_{kl}}{1+\Delta_{kl}}\right)(D_{kl}\{1 + e^{-\alpha_{kl}(R_{kl}-R^{eq}_{kl})}\}^2 - D_{kl}) \quad (6)$$

where Δ_{kl} is an adjustable Sato parameter[4] for the k–l interactions.

The "singlet" pseudopotential, E^1_{kM}, is given by the EAM expression:[2]

$$E^1_{kM} = F_k(\bar{\rho}_k(\mathbf{x})) + \sum_{j=N_s+1}^{N} \phi_{kj}(R_{kj}) \quad (7)$$

where $\bar{\rho}_k$ is the metal electron density at the location of the gas atom k and is approximated as a sum over atomic densities for all metal atoms in the system at the given point in space:

$$\bar{\rho}_k = \sum_{j=N_s+1}^{N} \rho^a_j(R_{kj}) \quad (8)$$

The embedding function F_k is the attractive component of the energy of embedding the nonmetal atom k into the homogeneous metal electron density $\bar{\rho}_k$. The pair repulsion, ϕ_{kj}, is the short-range Coulomb interaction between the nonmetal atom k and a particular metal atom j. It is given by

$$\phi_{kj} = Z_k(R_{kj})Z_j(R_{kj})/R_{kj} \quad (9)$$

where $Z_k(R)$ is the effective charge of atom k at distance R from the nucleus. The effective charge is an empirical function for a given type of atom.

The triplet pseudopotential is expressed as[1]

$$E^3_{kM} = h_{kM}(\bar{\rho}_k(\mathbf{x}))\{F_i(\bar{\rho}_k(\mathbf{x})) + \sum_{j=N_s+1}^{N} \phi_{kj}(R_{kj})\} \quad (10)$$

where $h_{kM}(\bar{\rho}_k)$ is an empirical scaling function, which is a geometry-dependent generalization of the Sato parameter in (6).

The potential energy function, V_{DIM}, is defined as the lowest energy obtained by solving the secular equation

$$\det |\mathbf{H} - \mathbf{S}V_{DIM}| = 0 \quad (11)$$

where **H** and **S** are the electronic Hamiltonian and overlap matrices of EDIM theory. The matrix elements of **H** are obtained from the diatomic potentials and pseudopotentials. The matrix elements of **H** and **S** for two or three univalent nonmetal atoms interacting with a metal surface are given in ref 1.

2.2. New Parametrization for Hydrogen Atoms on Ni Surfaces. Daw and Baskes[5] presented a parametrization of EAM for a single H adsorbed in Ni, Rice et al.[6] improved the parameters so that a single H adsorbed on the surface of Ni is also treated accurately, and the authors and Garrett[1] presented a parametrization of EDIM for the cases of one or two hydrogen atoms on the (100), (110), and (111) faces of Ni. In the present article we present some minor modifications to both the EAM and EDIM parameters in order to handle the cases of steps and three hydrogen atoms on a Ni surface. To differentiate the new parameters from the previous ones,[1,5,6] even though all parameters do not change with each new set, we refer to the new parameters as parameter set 4.

2.2.1. EAM Parametrization for H on Ni. In the present study, the empirical forms and parameters of the embedding energy, F_i, and pairwise repulsive interactions, ϕ_{ij}, in the EAM expression of the potential energy are taken to be the same as in the previous study,[1] except for N_s, which is the effective number of 4s electrons used[5,6] in calculating the Ni atomic density, and for $s(R)$, which is a smoothing function that occurs in the effective atomic charges, $Z(R)$, and in the atomic density, $\rho^a(R)$.

In the previous study,[1] we used different values of N_s for the metal atoms on the surrface than for those in the bulk, in order to improve the vertical out-of-plane vibrational frequency of a hydrogen atom adsorbed on a 4-fold site of the (100) face. However, this frequency is only improved by 10% by this change, which reduces it (in the harmonic approximation) from 750 to 690 cm^{-1}. Although the resulting frequency is in better agreement with the experimental value[7] of 600 cm^{-1}, the equilibrium height above the surface of a hydrogen at such a site is in worse agreement with the value deduced from experiment,[8] so the modification of N_s was only partially successful. However, making N_s different at the surface has the very unfortunate effect that when the surface has steps as in the present paper, it is not clear which value of N_s to use for metal atoms at the steps. Consequently, to allow unambiguous calculations on imperfect crystal faces, we decided in the present parametrization to use the same value of N_s on the surface as in the bulk, and we set N_s to the original[5,6] value, $N_s = 2$.

In the previous study,[1] the smoothing function $s(R)$ had the form

$$s(R) = \begin{cases} \exp(\eta/(R_c - R)) & R < R_c \\ 0 & R \geq R_c \end{cases} \quad (12)$$

where R_c is the cutoff radius and was set equal to 4.8 Å, and η is a damping parameter which had a value of 0.05. Preliminary dynamical calculations for the present application, however, showed that (12) has a deficiency, namely, that the derivative, $s'(R) = ds/dR$, of $s(R)$ has a maximum at $R = (R_c - \eta/2)$. The magnitude of the maximum is inversely proportional to η:

$$s'(R_c - \eta/2) = 4e^2/\eta \quad (13)$$

and, in fact, it is quite large for $\eta = 0.05$. As a result, it introduces unphysical features into the derivative of the function being smoothed in the vicinity of $R = R_c - \eta/2$. In the present study, we use a different smoothing function, which is defined as

$$s(R) = \begin{cases} 1 & R \leq R_c \\ \dfrac{R - (R_c + \Delta)}{-\Delta} - \dfrac{1}{2\pi}\sin\left[\pi\left(\dfrac{2R - 2R_c - \Delta}{\Delta}\right)\right] & R_c < R < R_c + \Delta \\ 0 & R_c + \Delta \leq R \end{cases} \quad (14)$$

where the cutoff radius R_c is set equal to 5 Å, and the smoothing interval Δ is also equal to 5 Å. The large smoothing interval guarantees that there is no spurious feature in the derivative of the function being smoothed. Furthermore, the smoothing function, $s(R)$ in (14), has been used without difficulty in one of our previous related dynamical studies.[9] Note that (14) has zero

(3) Ellison, F. O. *J. Am. Chem. Soc.* **1963**, *85*, 3540. Tully, J. C. In *Semiempirical Methods of Electronic Structure Calculations, Part A*; Segal, G. A., Ed.; Plenum: New York, 1977; p 173.
(4) Sato, S. *Bull. Chem. Soc. Jpn.* **1955**, *28*, 450; *J. Chem. Phys.* **1955**, *23*, 592, 2465.
(5) Daw, M. S.; Baskes, M. T. *Phys. Rev. B* **1984**, *29*, 6443.
(6) Rice, B. M.; Garrett, B. C.; Koszykowski, M. L.; Foiles, S. M.; Daw, M. S. *J. Chem. Phys.* **1990**, *92*, 775.
(7) Anderson, S. *Chem. Phys. Lett.* **1978**, *55*, 185.
(8) Stensgaard, I.; Jakobsen, F. *Phys. Rev. Lett.* **1985**, *54*, 711.
(9) Truong, T. N.; Hancock, G.; Truhlar, D. G. *Surf. Sci.* **1989**, *214*, 523.

TABLE I: EDIM Parameter Set 4[a]

EAM

$N_{s,s} = N_{s,b} = 2.0$

$$s(R) = \begin{cases} 1 & R < R_c \\ \dfrac{R - (R_c + \Delta)}{-\Delta} - \dfrac{1}{2\pi} \sin\left[\pi\left(\dfrac{2R - 2R_c - \Delta}{\Delta}\right)\right] & R_c \le R \le R_c + \Delta \\ 0 & R_c + \Delta < R \end{cases}$$

$R_c = 5.0$ Å $\quad \Delta = 5.0$ Å

EDIM

$\Delta_{H-H} = 0.13$

$A = 32.0 \quad B = 0.055 \quad C = 0.8$

[a] This table contains all parameters that differ from those in ref 1.

first and second derivatives at both R_c and $R_c + \Delta$. Consequently, the functions being smoothed are continuous through second derviatives. In the present study, we have used $s(R)$ defined by (14) in calculating the effective nuclear charges, $Z(R)$, and atomic densities, $\rho^a(R)$, for both Ni and H atoms. The final expressions for $Z(R)$ and $\rho^a(R)$ thus have the form

$$f(R) = F(R)\, s(R) \tag{15}$$

where $F(R)$ is the original unsmoothed[1] empirical form of $Z(R)$ or $\rho^a(R)$.

2.2.2. EDIM Parametrization for H_2 and H_3 on Ni. The EDIM parameters consist of the hydrogen–hydrogen Sato parameter, Δ_{H-H}, for the triplet H–H potential curve and the parameters A, B, and C of the scaling function $h(\bar{\rho})$ for the "triplet" H–Ni surface interactions. In the present study, we use the same empirical form for h as in our previous study:[1]

$$h(\bar{\rho}) = \tfrac{1}{2} \tanh\,[A(\bar{\rho} - B)] + C \tag{16}$$

However, the parameters A, B, and C are determined differently. We also use a different value for Δ_{H-H}.

First, we consider the Δ_{H-H} Sato parameter. In order to investigate the possibility of the exchange reaction $H + H'H'' \rightarrow HH' + H''$ on a metal surface, the EDIM potential energy function will be required to have an accurate barrier height for the gas-phase $H + H_2$ exchange reaction, and Δ_{H-H} is adjusted to achieve this. We set Δ_{H-H} equal to 0.13 (very similar to the value of 0.132 used in a previous[10] similar parametrization); $\Delta_{H-H} = 0.13$ yields a classical barrier height for the gas-phase exchange reaction of 9.94 kcal/mol and a zero-point-energy-corrected barrier of 9.12 kcal/mol. These values are close enough for our purposes to the values obtained from accurate surfaces.[11]

The parameters A, B, and C were determined from fitting to available experimental data for H_2 interacting with Ni surfaces. As in the previous study,[1] we adjust these parameters so that the dissociative chemisorption of H_2 has a barrier of about 1.2 kcal/mol on the Ni(100)[12] surface, no barrier on the Ni(110) surface,[13,14] and a barrier on the order of 2 kcal/mol on the Ni(111) surface.[13,14] Initially, we used the classical barrier of the lowest energy dissociative chemisorption path on each Ni surface for the above fitting purpose. However, preliminary dynamical calculations indicated that there is a large variational transition state effect for the dissociative chemisorption of hydrogen on all three low-index faces of Ni; i.e., in all three cases the maximum, ΔV_a^{AG}, of the vibrationally adiabatic ground-state potential energy curve[15-17] is significantly higher (about 0.5–0.6 kcal/mol) than the zero-point-energy-corrected barrier at the transition state. Therefore, we readjusted A, B, and C so that ΔV_a^{AG} barriers are consistent with experimental data. The final values of all parameters that have different values from the previous study[1] are given in Table I.

3. Dynamical Theory

3.1. Formulation. A general formalism for canonical variational transition state theory (CVT) for calculations of adsorbate dynamical processes at gas–solid interfaces has been described elsewhere.[9,18-23] In the present paper, we just summarize the most essential parts.

For a given reaction, we first calculate the minimum energy path (MEP) that connects the reactants (R) and products (P), via the saddle point (S) if it exists. If there is a saddle point, the MEP is found by following the paths of steepest descents from S to R and from S to P. If the saddle point does not exist, the method for calculating the MEP is different and is described below. The reaction coordinate s is then defined as the distance along the MEP, with its origin at the saddle point, with positive values of s on the product side, and with negative values of s on the reactant side.

At each distance s along the MEP, we define a generalized transition state (GTS) dividing surface orthogonal to the MEP in a mass-scaled Cartesian coordinate space. Each GTS is labeled by the value of s at which it interesects the MEP, and the generalized transition state rate constant at the temperature T is given by[17]

$$k^{GT}(T,s) = \frac{\sigma}{\beta h} \frac{Q^{GT}(T,s)}{\Phi^R(T)} e^{-\beta V_{MEP}(s)} \tag{17}$$

where σ is the symmetry factor, β is $(k_B T)^{-1}$, k_B is Boltzmann's constant, h is Planck's constant, $\Phi^R(T)$ is the quantal reaction partition function per unit volume evaluated at the overall zero of energy (which is set at the classical equilibrium geometry of the reactants), and $Q^{GT}(T,s)$ is the generalized transition state partition function evaluated with zero of energy at $V_{MEP}(s)$, which is the classical energy along the MEP at s relative to the overall zero of energy.

In canonical variational transition state theory (CVT),[24] the rate constant $k^{CVT}(T)$ is obtained by minimizing the generalized transition state rate constants with respect to s:

$$k^{CVT}(T) = \min_s k^{GT}(T,s) \equiv k^{GT}[T,s_*^{CVT}(T)] \tag{18}$$

For comparison the conventional transition state theory rate constant, $k^{TST}(T)$, can be calculated by setting $s = 0$ in (17). Note that all degrees of freedom orthogonal to the reaction coordinate are treated quantum mechanically in (17) and (18), but the reaction coordinate is treated classically.

For processes with barriers or effective barriers, quantal effects on the reaction coordinate, namely, tunneling, can be important. Tunneling contributions are taken into account by multiplying $k^{CVT}(T)$ by a ground-state transmission coefficient, $\kappa^{CVT/G}(T)$, which can be expressed as a ratio of the thermally averaged transmission probability $P^G(E)$ for total energy E to the thermally

(10) Thompson, D. L.; Blais, N. C.; Truhlar, D. G. *J. Chem. Phys.* **1983**, *78*, 1335.
(11) Truhlar, D. G.; Wyatt, R. E. *Adv. Chem. Phys.* **1977**, *36*, 141. Varandas, A. J. C.; Brown, F. B.; Mead, C. A.; Truhlar, D. G.; Blais, N. C. *J. Chem. Phys.* **1987**, *86*, 6258.
(12) Hamza, A. V.; Madix, R. J. *J. Phys. Chem.* **1985**, *89*, 5381.
(13) Robota, H. J.; Vielhaber, W.; Lin, N. C.; Segner, T.; Ertl, G. *Surf. Sci.* **1985**, *155*, 101.
(14) Steinrück, H. P.; Winkler, A.; Rendulic, K. D. *Phys. Rev. B* **1985**, *32*, 5032.
(15) Truhlar, D. G. *J. Chem. Phys.* **1970**, *53*, 2041.
(16) Garrett, B. C.; Truhlar, D. G.; Grev, R. S. In *Potential Energy Surfaces and Dynamics Calculations*; Truhlar, D. G., Ed.; Plenum: New York, 1981, p 587.
(17) Truhlar, D. G.; Isaacson, A. D.; Truhlar, D. G. In *Theory of Chemical Reaction Dynamics*; Baer, M., Ed.; CRC Press: Boca Raton, FL, 1985; Vol. IV, p 65.
(18) Lauderdale, J. G.; Truhlar, D. G. *J. Am. Chem. Soc.* **1985**, *107*, 4590.
(19) Lauderdale, J. G.; Truhlar, D. G. *Surf. Sci.* **1985**, *164*, 558.
(20) Lauderdale, J. G.; Truhlar, D. G. *J. Chem. Phys.* **1986**, *84*, 1843.
(21) Truong, T. N.; Truhlar, D. G. *J. Phys. Chem.* **1987**, *91*, 6229.
(22) Truong, T. N.; Truhlar, D. G. *J. Chem. Phys.* **1988**, *88*, 6611.
(23) Truong, T. N.; Truhlar, D. G.; Chelikowsky, J. R.; Chou, M. Y. *J. Phys. Chem.* **1990**, *94*, 1973.
(24) Garrett, B. C.; Truhlar, D. G. *J. Chem. Phys.* **1979**, *70*, 1593.

TABLE II: Binding Energies (kcal/mol), Heights above the Surface (a_0), and Vibrational Frequencies (cm^{-1}) of H on Clean (100), (110), and (111) Terraces of Ni

site	D_e	$\Delta H°_{298}$	Z_e	ν		
			H/Ni(100)			
4-fold	64.41 (63–66)[a]	−62.38	1.02 (0.95 ± 0.10)[b]	524	524	773 (597–629)[c]
bridge	60.30		1.80	293*i*	454	1280
atop	57.80		2.41	217*i*	217*i*	2284
			H/Ni(110)			
long bridge	64.31 (62)[d]	−62.33	0.37	215	593	862
3-fold	63.42	−61.32	0.59	181	267	1170
short bridge	59.81		1.74	236*i*	452	1293
long-bridge-to-3-fold TS[e]	63.39		0.56	175*i*	274	1200
center	63.30		0.53	191*i*	184*i*	1289
atop	57.40		2.38	212*i*	157*i*	2408
			H/Ni(111)			
hcp site	62.06 (63)[a]	−59.74	1.78 (2.2 ± 0.2)[e]	393	393	1176
fcc site	62.07 (63)[a]	−59.74	1.78 (2.2 ± 0.2)[e]	394	394	1180 (1120)[f]
bridge	61.19		1.90	276*i*	476	1290
atop	58.32		2.44	237*i*	237*i*	2191
			H/Ni(100) Step			
top of step	64.39	−62.41	0.04	239	542	897
bottom of step	65.22	−63.34	1.21	417	463	784
diffusion TS[g]	63.88		2.48	215*i*	202	1179

[a] References 31 and 32. [b] Reference 8. [c] References 7 and 36. [d] Reference 33. [e] Reference 34. [f] Reference 35. [g] TS denotes transition state.

averaged classical transmission probability for the ground-state (G) vibrationally adiabatic potential energy curve:[25]

$$\kappa^{CVT/G}(T) = \frac{\int_{E_0}^{\infty} P^G(E) e^{-\beta E}\, dE}{\int_{V_a^G[s=s_*^{CVT}(T)]}^{\infty} e^{-\beta E}\, dE} \quad (19)$$

where V_a^G is the adiabatic ground-state potential curve defined as

$$V_a^G(s) = V_{MEP}(s) + \epsilon_{int}^{GT}(s) \quad (20)$$

and ϵ_{int}^{GT} is the internal energy of the generalized transition state at s, s_*^{CVT} is defined by (18), and E_0 is the quantal threshold energy defined by

$$E_0 = \max\,[V_a^{RG}, V_a^{PG}] \quad (21)$$

where V_a^{RG} and V_a^{PG} are the values of V_a^G at the reactants and products, respectively.

The ground-state transmission probability $P^G(E)$ for the total energy E is approximated by the small-curvature semiclassical (SCS) adiabatic ground-state (AG) approximation, and its mathematical form is given elsewhere.[26] This approximation incorporates the effect of reaction path curvature by using local s-dependent effective reduced mass, μ_{eff}, and the final resulting rate constant is denoted as $k^{CVT/SCSAG}$. If the reaction path curvature effect is neglected, which corresponds to assuming that the best tunneling path is the MEP, the rate constant is denoted as $k^{CVT/M\text{-}EPSAG}$.

For processes for which V_a^G does not have an intrinsic barrier (i.e., the maximum occurs at the reactants or products), we neglect quantal effects on the reaction coordinate. However, in this case, we multiply k^{CVT} by the nonvariational classical adiabatic ground-state (CAG) transmission coefficient,[25] $\kappa^{CVT/CAG}$, that accounts for the classical reflection of trajectories below the barrier of the adiabatic ground-state potential curve:

$$\kappa^{CVT/CAG}(T) = \exp(-\beta\{V_a^{AG} - V_a^G[s=s_*^{CVT}(T)]\}) \quad (22)$$

where V_a^{AG} is the maximum of the V_a^G curve:

$$V_a^{AG} = \Delta V_a^{AG} + \epsilon_{int}^R \quad (23)$$

where ϵ_{int}^R being the internal energy at the reactants. The corresponding rate constant is denoted as $k^{CVT/CAG}$.

3.2. Computation Details. All calculations were performed with the use of POLYRATE program, version 1.5.[27]

Both for processes with a saddle point and for those without one, the MEP is computed by following the steepest descent path using the Page–McIver method[28] with a step size of 0.01 a_0. A difference between these types of reactions, though, is in the initial point and initial step for this calculation. For reactions that have a barrier, the steepest descent path is started from the saddle point, the first step in each direction is along the imaginary-frequency normal mode, and the path is followed to both reactants and products. However, for $H_2(g) \rightarrow H_2(a)$, where $H_2(a)$ denotes the molecule in a physisorbed state, there is no barrier, so the MEP is started with H_2 at a large but finite distance R_0 from the surface, and followed only in the inward direction. Then R_0 is increased until the MEP is converged over its significant portion.

In the present study, the Ni lattice is assumed to be rigid with the experimental lattice constant $a = 3.52$ Å.[29] For calculations on the (100) face, the lattice is modeled by a total of 817 atoms. This model has 9 layers, and the number of Ni atoms in each layer, from the top (surface) layer down, is 129, 120, 121, 112, 101, 88, 69, 52, and 25. The Ni(110) surface is modeled by 797 Ni atoms, and the number in each layer is 89, 84, 89, 84, 89, 76, 65, 64, 55, 44, 31, 20, and 11. The Ni(111) surface is represented by 828 Ni atoms, and the number in each layer is 151, 141, 141, 121, 102, 84, 61, and 27. Finally, the single-layer step of the Ni(100) surface is constructed by adding half a layer of Ni atoms such that the step lies along the [$\bar{1}$00] direction. Thus, in these calculations the metal is modeled by 881 Ni atoms, corresponding to a 64-atom half-layer on the top of the original 817-atom model. Note that the number of Ni atoms used to represent the metal is large enough to assure that both the fitting parameters discussed in the previous section and the dynamical results presented below are converged ith respect to the size of the lattice model.

The partition functions in (17) are evaluated by standard techniques. The electronic partition function of the metal is

(25) Garrett, B. C.; Truhlar, D. G.; Grev, R. S.; Magnuson, A. W. *J. Phys. Chem.* **1980**, *84*, 1730.

(26) Skodje, R. T.; Truhlar, D. G.; Garrett, B. C. *J. Phys. Chem.* **1981**, *85*, 3019.

(27) Isaacson, A. D.; Truhlar, D. G.; Rai, S. N.; Hancock, G. C.; Lauderdale, J. G.; Truong, T. N.; Joseph, T.; Garrett, B. C.; Steckler, R. University of Minnesota Supercomputer Institute Research Report UMSI 88/87, September 1988. An earlier version of this program, which is not applicable to reactions at surfaces is described in: Isaacson, A. D.; Truhlar, D. G.; Rai, S. N.; Steckler, R.; Hancock, G. C.; Garrett, B. C.; Redmon, M. J. *Comput. Phys. Commun.* **1987**, *47*, 91.

(28) Page, M.; McIver, J. W., Jr. *J. Chem. Phys.* **1988**, *88*, 922.

(29) Kittel, C. *Introduction to Solid State Physics*, 5th ed.; Wiley: New York, 1976.

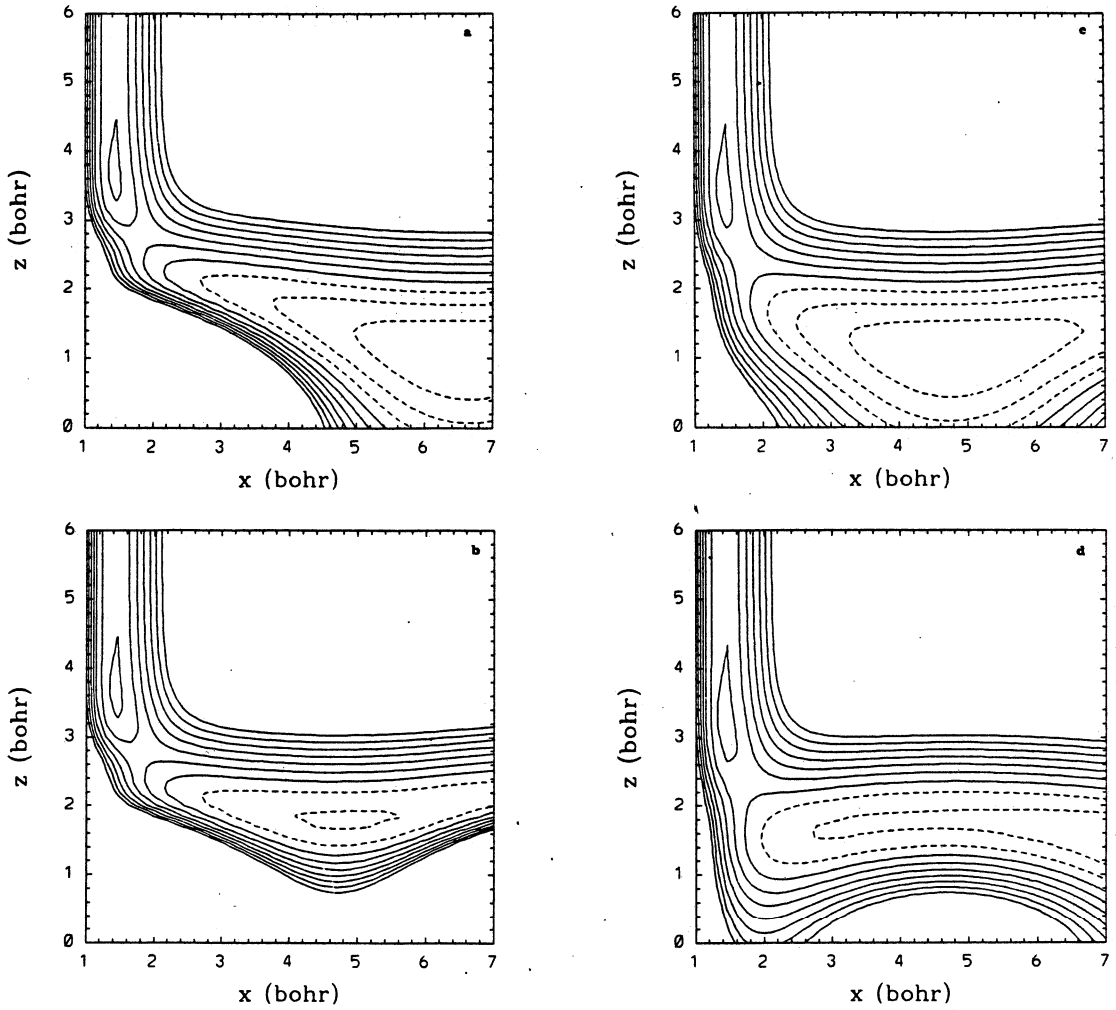

Figure 1. EDIM potential energy contours for the dissociative chemisorption of H_2 on a clean terrace of Ni(100), plotted against the H_2 bond distance r (in a_0) and the distance z (in a_0) of the center of mass of H_2 above the surface plane. The dashed contours correspond to negative values, and the solid contours correspond to positive ones or zero; the contour interval is 5 kcal/mol. The zero of energy corresponds to H_2 infinitely far from the surface. (a) The atop-to-center process with the center of mass and orientation of H_2 corresponding to structures T1, T2, and C2 of Figure 4. Contour levels are from −15 to 30 kcal/mol. (b) The atop-to-bridge process with the center of mass and orientation of H_2 corresponding to the T3, T4, and T5 structures. Contour levels are from −10 to 30 kcal/mol. (c) The bridge-to-center process with the center of mass and orientation of H_2 corresponding to the C1 structure. Contour levels are from −15 to 30 kcal/mol. (d) The center-to-center process with the center of mass and orientation of H_2 corresponding to the P1, T6, and C3 structures. Contour levels are from −10 to 30 kcal/mol.

assumed to cancel in the numerator and denominator. Furthermore, all vibrations are treated as harmonic. Although the harmonic approximation is not quantitatively reliable for the hindered translations and hindered rotations in early segments of the chemisorption reaction paths, it provides useful enough accuracy at the saddle point and variational transition states which are our primary concern. Rotations are treated classically without symmetry numbers,[17] and σ is taken to be 1 in all cases.

4. EDIM Potential Energy Function for H and H_2 on Ni

The newly parametrized EDIM potential energy functions (PEF) for H and H_2 on various faces of Ni are discussed in this section. Static properties of the binding sites of single H atom are given in Table II. Contours plots for dissociative chemisorption of H_2 above various sites of Ni surfaces are given in Figure 1 for the (100) face, Figure 2 for the (110) face, and Figure 3 for the (111) face. In these plots, the abscissa is the H–H bond distance, r, and ordinate is the height, z, of H_2 above the surface plane. For plotting purposes only the H_2 molecule is restricted to dissociate parallel to the surface plane and directly above a prespecified site (i.e., H_2 has a fixed orientation and fixed x, y coordinates for its center of mass). In Figures 4, 5, and 6, we present schematic diagrams that connect the main stationary points on paths leading to dissociative chemisorption of H_2 on the Ni-(100), -(110), and -(111) surfaces, respectively. The geometries given in Figures 4–6 are fully optimized in all six degrees of freedom, and normal-mode analyses were carried out at all stationary points to characterize the stationary points. The energy values given below the structures in Figures 4–6 are all relative to the energy of H_2 at its classical equilibrium bond distance and at an infinite distance above the surface. Thus, the relative energy at the saddle point or transition state is the classical barrier height for dissociative chemisorption of gas-phase H_2 at that point, and the binding energy of H_2(a) or 2H(a) on the Ni surface at each structure, relative to H_2(g), is the negative of its relative energy in Figures 4–6. The lowest energy or preferred dissociative chemisorption path on each face of the Ni crystal is indicated in each figure by the solid line that connects all stationary points along this path. The MEP and generalized normal mode analyses along the preferred dissociative chemisorption path are calculated in order to obtain the vibrationally adiabatic ground-state potential energy curve, V_a^G, defined by (20). Then the effective barrier height $\Delta V_a^{\ddagger G}$ for dissociation along the preferred path is given in the middle of the solid line segment that also indicates between which two stationary points the variational transition state occurs. Note that ΔV_a^{AG} differs from $\Delta V_a^{\ddagger G}$ quantity which was used to characterize dissociative paths in the previous study[1] in that ΔV_a^{AG} is the maximum of the ΔV_a^G curve while $\Delta V_a^{\ddagger G}$ is the value of the ΔV_a^G curve at $s = 0$, where

$$\Delta V_a^G(s) = V_a^G(s) - V_a^{RG} \qquad (24)$$

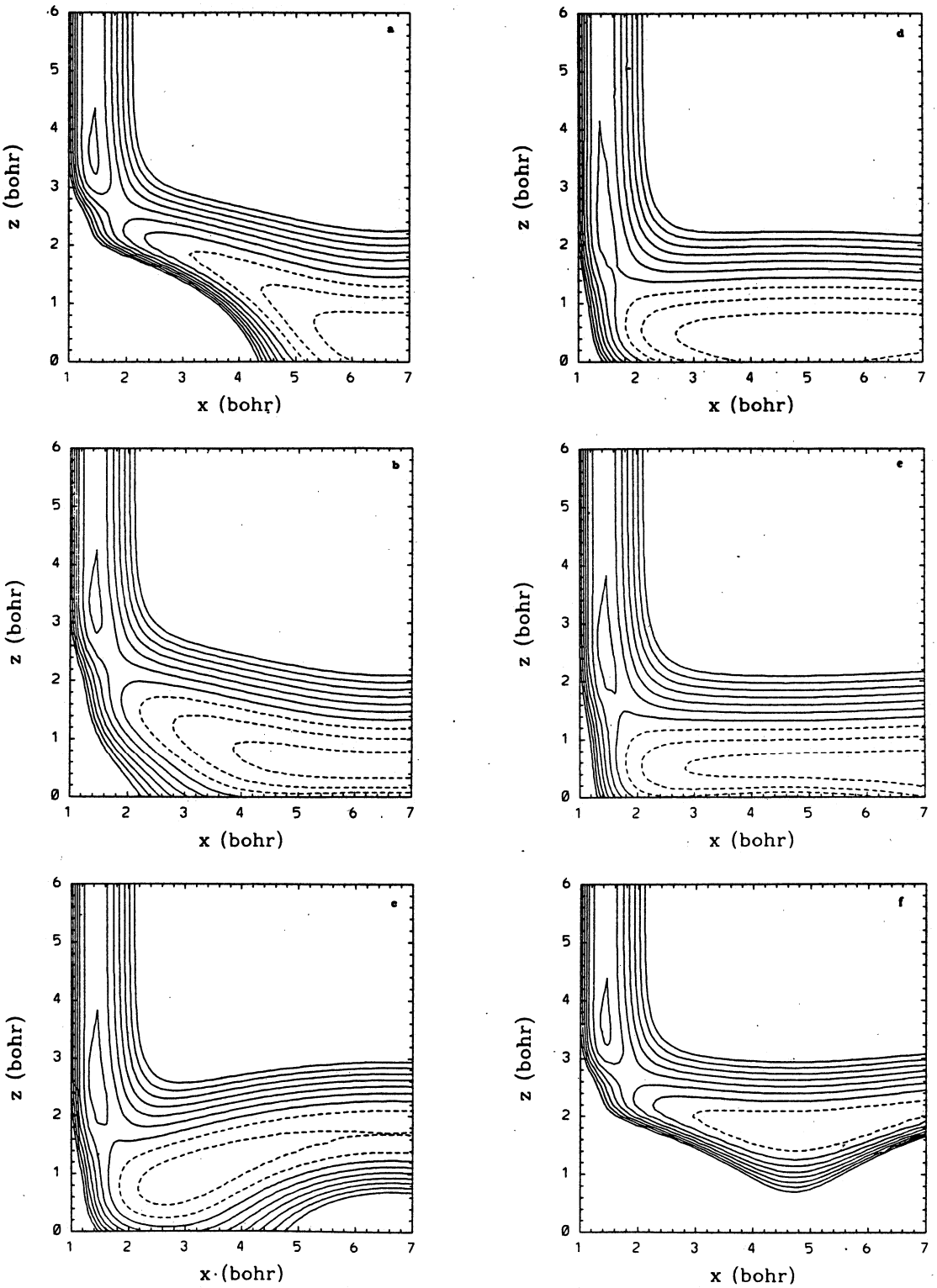

Figure 2. Similar to Figure 1 except for the dissociation of H_2 on the Ni(110) surface. (a) The atop-to-long-bridge process, with the center of mass and orientation of H_2 corresponding to the T7, T8 and C5 structures of Figure 5. Contour levels are from −15 to 30 kcal/mol. (b) The short-bridge-to-3-fold process with the center of mass and orientation of H_2 corresponding to the S3, T9, and C6 structures. Contour levels are from −15 to 30 kcal/mol. (c) The center-to-3-fold process with the center of mass and orientation of H_2 corresponding to the S4, S5, and C7 structures. Contour levels are from −10 to 30 kcal/mol. (d) The center-to-long-bridge process with the center of mass and orientation of H_2 corresponding to the P2, S2, and C4 structures. Contour levels are from −15 to 30 kcal/mol. (e) For the long-bridge-to-long-bridge process with the center of mass and orientation of H_2 corresponding to the S6, T10, and C8 structures. Contour levels are from −15 to 30 kcal/mol. (f) For the atop-to-short-bridge process with the center of mass and orientation of H_2 corresponding to the T11, T12, and T13 structures. Contour levels are from −5 to 30 kcal/mol.

[the reactant symbol R always refers to H_2(g) and never to H_2(a)].

The dashed lines in Figures 4–6 are the higher energy dissociation paths, whereas the dotted lines are the diffusion paths with the classical barriers relative to the specified zero of energy (i.e., H_2 infinitely far above the surface) listed in the middle of these dotted lines.

For the convenience of the following discussion, we refer to a structure in Figures 4–6, 9, and 12 as a precursor (P) state only if it has all real vibrational frequencies, one of which corresponds to an H–H stretching mode with a frequency close to that of free gas-phase H_2, and the rest of which have small frequencies corresponding to the hindered translational and rotational motions

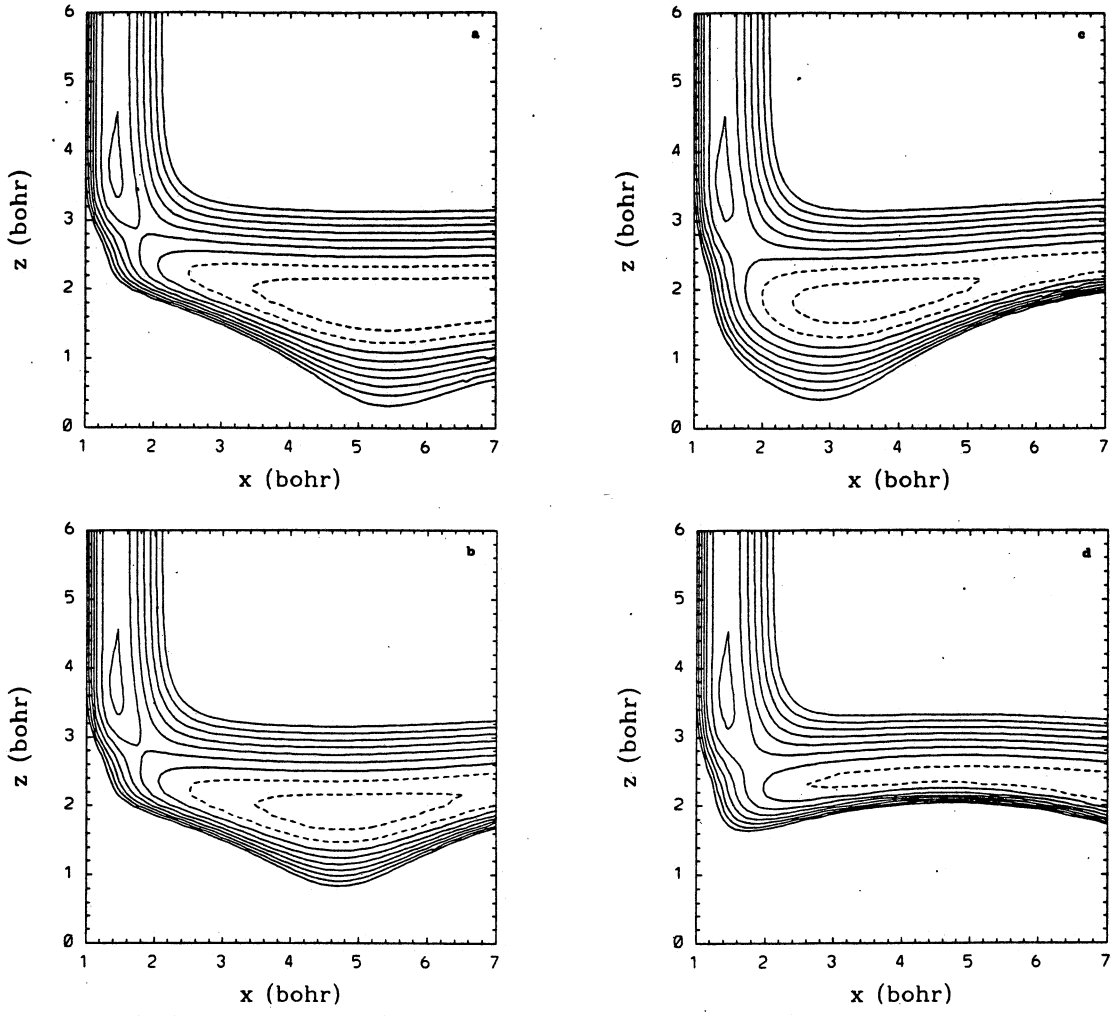

Figure 3. Similar to Figure 1, except for the dissociative chemisorption of H_2 on Ni(111). (a) The atop-to-bridge process with the center of mass and orientation of H_2 corresponding to the T14, T15, and T16 structures of Figure 6. Contour levels are from −10 to 30 kcal/mol. (b) The atop-to-center process with the center of mass and orientation of H_2 corresponding to the T17, T18 and C10 structures. Contour levels are from −10 to 30 kcal/mol. (c) The bridge-to-center process with the center of mass and orientation of H_2 corresponding to the S7 and C9 structures. Contour levels are from −10 to 30 kcal/mol. (d) The double-bridge-to-center process with the center of mass and orientation of H_2 corresponding to the C11 structure. Contour levels are from −5 to 30 kcal/mol.

of a weakly adsorbed H_2 molecule. (As mentioned in the previous study,[1] the above criteria are not sufficient to conclude that such a precursor state may be dynamically stabilized or experimentally observable, but they do single out potential surface features that may be responsible for such observable or dynamically significant precursor states.) Other stationary points with all real frequencies corresponding to nearly independent adsorbed hydrogen atoms and with geometries corresponding to chemisorbed atoms are denoted C. Transition states that have only one imaginary frequency are denoted S (saddle), while others with more than one imaginary frequency are denoted T (hilltop or higher order transition state).

4.1. H/Ni. The only differences in the EAM part of the EDIM PEF from the previous parameter set[1] are in N_s, the effective number of Ni 4s electrons, and in the form of the smoothing function. In the new parameter set, the effective number of 4s electrons is the same for Ni atoms in the surface layer and in the bulk and is equal to 2,[6] whereas N_s is slightly different for surface and subsurface metal atoms in the original[1] EDIM. In addition, the new smoothing function is physically better behaved. Overall, these differences are small; thus we expect that the new EAM PEF for H on Ni is quite similar to the previous one.[1] The equilibrium binding energies, the standard heat of adsorption at 298 K ($\Delta H°_{298}$), the equilibrium binding heights, and the vibrational frequencies for an H atom adsorbed on various sites of Ni(100), -(110), and -(111) faces are given in Table II. The standard heat of adsorption at temperature T is computed by use of the equation[30]

$$\Delta H°_T = D_e + \sum_{i=1}^{3} \frac{R\Theta_i}{e^{\Theta_i/T} - 1} - \frac{3}{2}RT \qquad (25)$$

where Θ_i is the characteristic vibrational temperature of mode i and is defined as $h\nu_i/k_B$, and R is the gas constant. The table shows that the binding energies of H atoms on various sites of Ni(100), -(110), and -(111) surface are slightly larger for the new parameter set than for the previous one, although the binding energies are still within experimental uncertainty,[31-33] and the lowest classical diffusion barriers for H on each face of the above three Ni faces are not significantly different for the two parameter sets. Furthermore, the equilibrium binding heights for H on the Ni(100), -(110), and -(111) surfaces are somewhat larger for the present case, and thus they are in better agreement with experimental values,[8,34] whereas the agreement with the experimental vibrational frequencies, overall, is about the same. In particular, for the new EDIM parameter set, the predicted vertical vibrational

(30) McQuarrie, D. A. *Statistical Mechanics*; Harper and Row: New York, 1976.
(31) Lapujoulade, J.; Neil, K. S. *Surf. Sci.* **1973**, *35*, 288; *J. Chem. Phys.* **1972**, *57*, 3535.
(32) Christmann, K.; Schober, O.; Ertl, G.; Neumann, H. *J. Chem. Phys.* **1974**, *60*, 4528.
(33) Engel, T.; Rieder, K. H. *Surf. Sci.* **1981**, *109*, 140.
(34) Christmann, K.; Behm, R. J.; Ertl, G.; Van Hove, M. A.; Weinberg, W. H. *J. Chem. Phys.* **1979**, *70*, 4168.

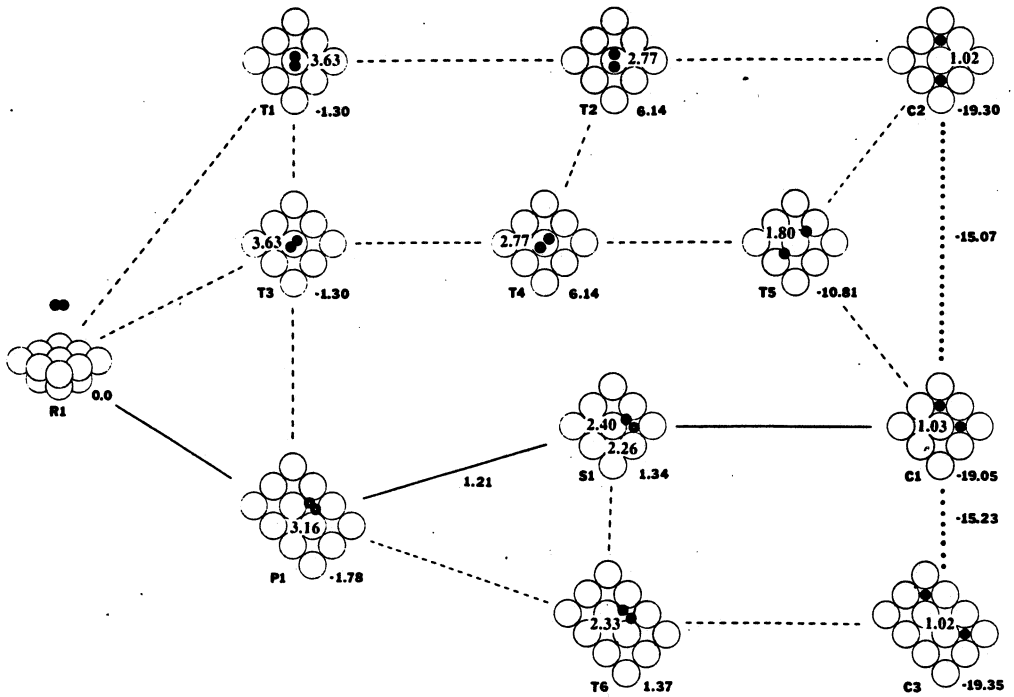

Figure 4. Schematic energy diagram for different dissociative chemisorption pathways that connect projections of the stationary point geometries on the *xy* plane for dissociative chemisorption of H_2 on a clean terrace Ni(100). The small dark spheres indicate the positions of the hydrogen atoms, and numerical values next to them are their distance (in a_0) above the surface plane (one value means that the distances are the same for both hydrogens). From the top to bottom of the figure are the atop-to-center, atop-to-bridge, bridge-to-center, and center-to-center processes. The prefixes of the geometry indices are defined as follows: P, physisorbed state (H_2 adsorbed as an undissociated molecule); S, saddle point (the Hessian matrix has one and only one imaginry eigenvalue); T, higher order transition state, also called a hilltop (the Hessian matrix has more than one imaginary eigenvalue); and C, chemisorbed state (dissociative product of two adsorbed H atoms). The solid lines are the minimum energy paths, the dashed lines are higher energy reaction paths involving higher order transition states, and the dotted lines are surface diffusion paths. The numerical value at midpoints of the dotted lines are the classical potential energy at the diffusion saddle point which converts between two states. All numerical values are the classical energy of the H_2/Ni(100) system at the geometry shown relative to the overall zero of energy which is set at the infinite separation of H_2 from the surface, except that the value at the midpoint of a solid line is the vibrationally adiabatic ground-state potential energy barrier, ΔV_a^{AG}, with respect to the zero-point energy of the equilibrium gas-phase H_2 molecule.

frequency of an H atom at a stable 4-fold site of Ni(100) is worse, while for an H atom at a stable 3-fold site of Ni(111), the vibrational frequency is in better agreement with experimental data[7,35,36] (see Table II). In conclusion, the present results confirm our expectation that the EAM part of the new EDIM PEF has very similar features to those found previously.

4.2. H_2/Ni(100). Dissociation of H_2 on Ni(100) has four possible paths, and we refer to them in order from the top row down in Figure 4 as the atop-to-center, atop-to-bridge, bridge-to-center, and center-to-center dissociation paths, or in Roman numerical order as processes I to IV, respectively. The two-dimensional energy contour plots are given in Figure 1a, 1b, 1c, and 1d, respectively. (In principle there are two additional possible dissociation paths, namely, the center-to-atop and bridge-to-atop paths; however, both lead to energetically unfavorable products and thus they are not considered.)

In general, the present EDIM potential energy functions for the dissociation of H_2 on Ni(100) are qualitatively similar to those of the previous study.[1] In particular, all dissociation processes on Ni(100), I–IV, pass through a stationary point in the physisorbed region. For dissociations over an atop site, such as the atop-to-center and atop-to-bridge processes, these stationary points, where H_2 resides about 3.6 a_0 above an atop site, are in fact transition states which then convert to the local minimum corresponding to the precursor state P1 with the binding energy of 1.78 kcal/mol and H_2 located at about 3.2 a_0 above a 4-fold (center) site. Furthermore, when H_2 dissociates over an atop site as in processes I and II, it must surmount a substantial barrier of the order of 6 kcal/mol, whereas if it dissociates over a bridge site, as in the bridge-to-center path, or over a center site, as in the center-to-center dissociation path, the barrier is much lower by nearly a factor of 5. The two lower barrier dissociation paths, the bridge-to-center and center-to-center processes, both have about the same barrier height, although the barrier for the bridge-to-center dissociation is lowest, with the classical barrier height being 1.34 kcal/mol. Including the zero-point-energy correction at the saddle point S1 yields a $\Delta V_a^{\ddagger G}$ barrier of only 0.5 kcal/mol. However, the vibrationally adiabatic ground-state barrier, ΔV_a^{AG}, is 1.21 kcal/mol, which should be compared with Hamza and Madix's[4] experimental observations, which they interpreted as tunneling through an effective barrier of 1.2 kcal/mol. Thus, if we assume the experimental interpretation is correct, the use of the $\Delta V_a^{\ddagger G}$ barrier in fitting the EDIM parameters in the previous study[1] would result in an overestimation of the true effective barrier ΔV_a^{AG}.

Both the bridge-to-center and center-to-center dissociation paths proceed through the same precursor state, P1; however, the preferred path, the bridge-to-center process, breaks its symmetry in that the hydrogen molecule does not remain horizontal above the surface plane along the MEP. For instance, at the saddle point structure S1, one hydrogen atom is located 2.26 a_0 above a center site in the surface plane and the other resides at 2.40 a_0 above a point in the surface plane near the neighboring bridge site. Eventually as the reaction proceeds, this hydrogen atom moves across the bridge site to form the chemisorption state C1, where both hydrogens are adsorbed at 1.03 a_0 above two nearest center sites and have a binding energy of 19.05 kcal/mol.

On the other hand, the center-to-center process retains its symmetry along the MEP, and at the transition state T6, the two hydrogen atoms are located 2.33 a_0 symmetrically above a center site. The classical barrier for this process is only 0.04 kcal/mol higher than that of the preferred path. Furthermore, normal-model analysis at the transition state, T6, of the center-to-center

(35) Ho, W.; DiNardo, N. J.; Plummer, D. E. *J. Vac. Sci. Technol.* **1980**, *17*, 314.
(36) Karlsson, P. A.; Martensson, A.-S.; Andersson, S.; Nordlander, P. *Surf. Sci.* **1986**, *175*, L759.

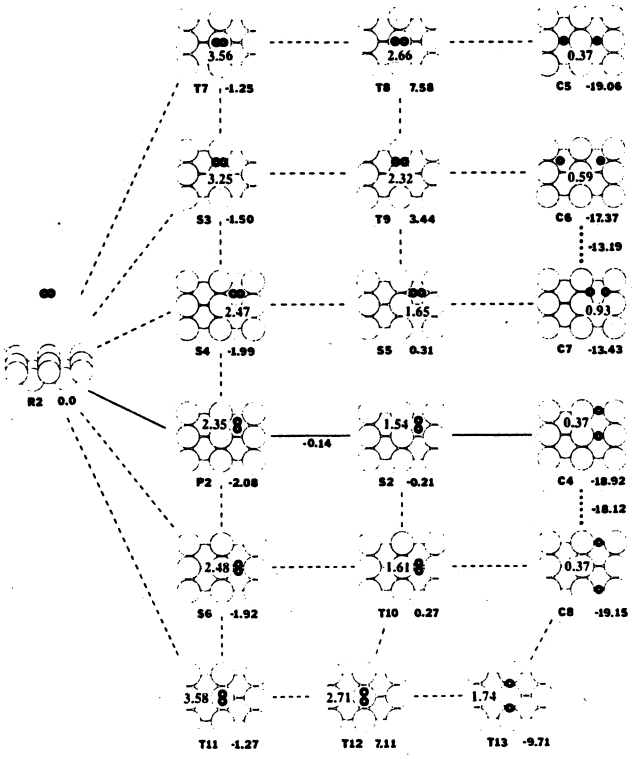

Figure 5. Same as Figure 4, except for H_2 dissociating on a clean terrace of Ni(110). From the top down are the atop-to-long-bridge, short-bridge-to-3-fold, center-to-3-fold, center-to-long-bridge, long-bridge-to-long-bridge, and atop-to-short-bridge processes, respectively.

process yields two imaginary frequencies; one corresponds to the dissociation of H_2, and the other to motion toward the saddle point (S1) of the preferred path. Thus, the bridge-to-center and center-to-center dissociation paths might be dynamically coupled; however, further study of this interesting dynamical question is beyond the scope of the present paper.

It is interesting to compare our results with the recent experiment of Zhu and White.[37] In the present study, the heat of adsorption, ΔH°_0, for H_2 on the Ni(100) surface calculated from the preferred dissociation path is 20.97 kcal/mol, which is about the average of the experimental values[37] of 19.1 ± 0.3 and 22.7 ± 0.4 kcal/mol that are calculated from different models. Furthermore, the effective barrier, ΔV_a^{AG}, for desorption of hydrogen from Ni(100) calculated from the preferred path (C1 → S1 → P1 → R1) is predicted to be 22.18 kcal/mol, and it can be compared with the experimental activation energy of 22.7 ± 0.2 kcal/mol[37] for the temperature range from 300 to 340 K. These results indicate that the present EDIM PEF is not only accurate in the entrance channel but also accurate in the exit channel, and thus they are very encouraging.

In addition, the recent experimental study of Zhu et al.[38] reported evidence for the coexistence of direct and precursor dynamics in the dissociative chemisorption of H_2 on Ni(100). In particular, the experimenters concluded that a direct dissociative channel dominates above 200 K, whereas a precursor-mediated channel makes a measurable contribution below 200 K. The authors[38] proposed that the precursor-mediated channel occurs at surface defects such as steps or kinks. In a later section we discuss the effect of surface defects, namely, a step, on the dissociative chemisorption process. Here, we provide other possible explanations for the above experimental observation. One possible explanation that had been suggested in our previous study[9] is that direct processes such as dissociations over an atop site generally have large barriers, but yield thermodynamically more stable products so they are thermodynamically more favorable at high temperatures; whereas precursor-mediated processes have much lower barriers, so although they yield thermodynamically less stable products, they are kinetically more favorable at low temperatures. This explanation is also consistent with the present new calculations, although the differences in the stability of the chemisorption products from both direct and precursor-mediated processes are less profound. It is also possible that both direct and precursor-mediated channels coexist along a single dissociation path. This can be rationalized as follows. The precursor state, if it exists, may bind only very weakly to the surface. In particular, for the H_2/Ni(100) system, Zhu et al.[38] reported that the surface temperature dependence of the initial sticking probability disappears above 200 K. This may indicate that the binding energy of the precursor is of order 1 kcal/mol or less. Under thermal equilibrium conditions such as in the Zhu et al.[38] experiment, H_2 gas molecules have a Boltzmann distribution of kinetic energy. Thus at high temperatures, most of the H_2 gas-phase molecules have kinetic energy sufficiently above the barrier to chemisorption; hence they would not be appreciably affected by the shallow well (precursor state) on the potential energy surface in the entrance channel. Consequently, the dissociation of H_2 on Ni(100) may behave as a direct process. On the other hand, at low temperatures, some H_2 gas-phase molecules do not have sufficient kinetic energy to surmount the barrier to chemisorption; however, they have sufficient time to be equilibrated and trapped in these precursor states. Once trapped in the physisorbed well, adsorbed H_2 molecules require more kinetic energy to dissociate than free H_2 molecules would. As a consequence, the precursor-mediated processes may make some contribution to the total dissociative probability at the low temperatures studied by Zhu et al.[38] Although this latter possibility provides a reasonable explanation for the experimental observations,[37] the argument given by Zhu et al.[38] is also consistent with the present results as seen below.

4.2. H_2/Ni(110). For H_2 on the (110) surface of Ni, we found six possible dissociation paths, and we refer to them from the top row down in Figure 5 as the atop-to-long-bridge, short-bridge-to-3-fold, center-to-3-fold, center-to-long-bridge, long-bridge-to-long-bridge, and atop-to-short-bridge processes, or in Roman numerical order as processes V, VI, VII, VIII, IX, and X, respectively. The energy contour plots for processes V, VI, VII, VIII, IX, and X are given in Figure 2a, 2b, 2c, 2d, 2e, and 2f, respectively. As in the case of H_2 on Ni(100), there are more possible dissociation paths for H_2 on Ni(110). However, we found that these paths either lead to energetically unstable products (such as both hydrogen atoms adsorbed on atop sites) or the stationary points do not even exist on the EDIM PEF. Therefore, the six dissociation paths in Figure 5 are the only dynamically important reaction paths for the present EDIM PEF.

In all cases considered, the hydrogen molecule dissociates horizontally above the indicated site (i.e., the x and y coordinates of the center of mass of H_2 remains constant along the path), and H_2 either orients perpendicular to the valley in the direction [001] as in processes V to VII, or along the valley in the direction [1$\bar{1}$0] such as in processes VIII to X. In addition, all dissociating hydrogen molecules pass, on the minimum energy paths, through a stationary physisorbed state with a binding energy in the range from 1.25 to 2.08 kcal/mol. One of these six stationary points is the precursor state, P2, which is the most strongly bound precursor structure, while others are either saddle points or transition states which have at least one downhill direction that leads to this P2 local minimum. The P2 precursor state has the hydrogen molecule 2.35 a_0 above a center site, which is closer than the distance above the surface plane at the other physisorbed states. As in the case for H_2 on Ni(100), dissociation of H_2 over an atop site such as in the atop-to-long-bridge, process V, or atop-to-short-bridge, process X, has a substantial classical barrier; it is of order 7–8 kcal/mol. As observed in our previous study,[1] the closer the H_2 can get to the surface plane at the transition state, the more attractive the adsorbate–metal interactions become; although repulsive interactions also increase, this tends to lower the classical barrier height. As shown in Figure 5, the preferred path is the center-to-long-bridge dissociation with a classical barrier

(37) Zhu, X.-Y.; White, J. M. *J. Phys. Chem.* **1988**, *92*, 3970.
(38) Zhu, X.-Y.; Castro, M. E.; White, J. M. *J. Chem. Phys.* **1989**, *90*, 7442.

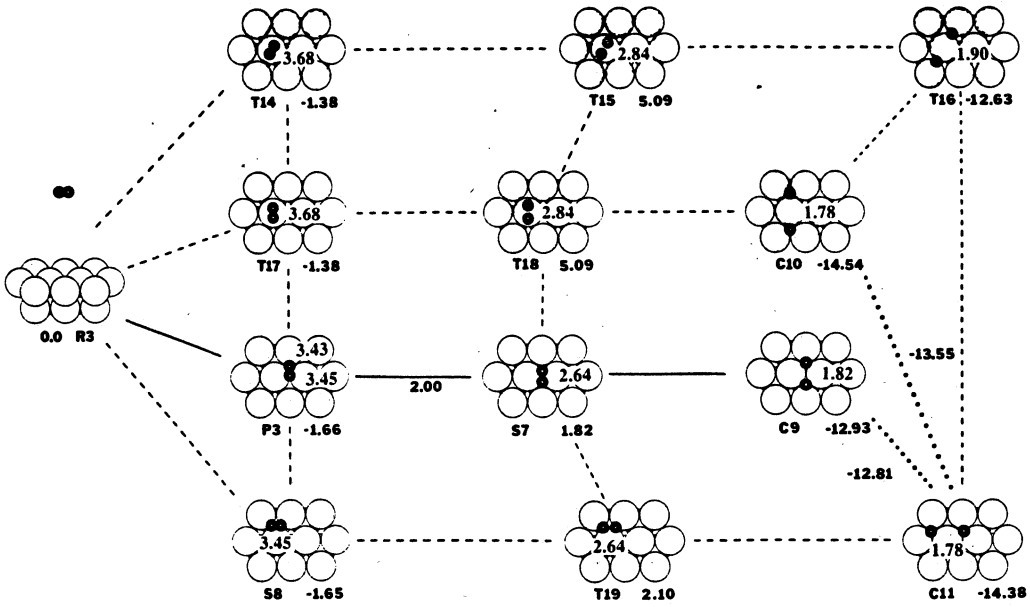

Figure 6. Same as Figure 4 except for H_2 dissociating on a clean terrace of Ni(111). From the top down are the atop-to-bridge, atop-to-center, bridge-to-center, and double-bridge-to-center processes, respectively.

of −0.21 kcal/mol; that is, the saddle point is actually 0.21 kcal/mol below the energy of H_2 at infinity. The vibrationally adiabatic ground-state barrier, ΔV_a^{AG}, for this process is −0.14 kcal/mol, which means it is 0.14 kcal/mol below the internal energy of the reactant. In other words, the dissociation of H_2 on Ni(110) occurs without activation, which is consistent with experimental observations of Robota et al.[13] and Steinrück et al.[14]

The other two low-barrier dissociation paths are the long-bridge-to-long-bridge process, with a classical barrier of 0.27 kcal/mol, and the center-to-3-fold process, with a classical barrier of 0.31 kcal/mol. Both have the transition state located above the valley, and the hydrogen molecule at these transition states, T10 and S5, is closer to the surface plane than at the transition states of other higher barrier processes. Notice that the chemisorption product, C7, of the center-to-3-fold process is stable with a binding energy of 13.43 kcal/mol, even though the two hydrogen atoms are only 3 a_0 apart. This is different than what we found in our previous study[1] where this product is only metastable due to H–H repulsion. This change is a direct consequence of making the Δ_{H-H} Sato parameter larger here, which decreases the H–H repulsion in the present EDIM PEF. Also, as another consequence of this change, the chemisorption states of the present EDIM PES have higher binding energies than those of the previous study.[1]

4.3. H_2/Ni(111). For H_2 on Ni(111), we found four possible dissociation paths, and we refer to them from the top row down in Figure 6 as the atop-to-bridge, atop-to-center, bridge-to-center, and double-bridge-to-center dissociations or in Roman numerical as order processes XI, XII, XIII, and XIV, respectively. As in the earlier sections, there are additional possible dissociation paths; however, they lead to energetically very unstable products and thus are less important and not included in the present discussion.

As in the dissociation of H_2 on the other two faces of Ni, all processes considered here go through a physisorbed state. In this case the binding energies range from 1.38 to 1.66 kcal/mol. The stable precursor state P3 has the largest binding energy, while other physisorbed states are either a saddle point or transition states which can lead to the local minimum, P3. The precursor state P3 has one hydrogen atom adsorbed 3.43 a_0 above a center site, and the other atom is 3.45 a_0 above the plane close to the nearby bridge site, but the other physisorbed states have the H_2 oriented horizontally and symmetrically above the site upon which it dissociates. The geometry of the precursor state P3 is consistent with what Russell et al.[39] postulate in explaining their experimental data for D_2 on Ni(111).

Similarly to H_2 on Ni(100) and Ni(110), dissociation of H_2 over an atop site of Ni(111) has a large barrier such as for the atop-to-center and atop-to-bridge processes, while dissociation processes of H_2 over a bridge site or over two neighboring bridge sites, such as in the bridge-to-center or double-bridge-to-center processes, respectively, have significantly lower classical barriers.

The preferred path for the dissociation of H_2 on Ni(111) is the bridge-to-center process which proceeds via the precursor state P3 over the saddle point S7 to yield the chemisorption state C9 The classical barrier for this process is 1.82 kcal/mol. Including a zero-point-energy correction at the transition state lowers the barrier to 1.54 kcal/mol. However, the vibrationally adiabatic ground-state potential barrier, ΔV_a^{AG}, is 2.0 kcal/mol, which is in good agreement with experimental data of Robota et al.,[13] which indicate a barrier of about 2 kcal/mol, and of Steinrück et al.[14], which indicate an effective barrier of order 1–2 kcal/mol. Note that the saddle point S7 regains its symmetry and has H_2 located 2.64 a_0 above a bridge site. The bridge-to-center chemisorption product differs from the previous study[1] in that it is stable and has a binding energy of 12.93 kcal/mol. The double-bridge-to-center path has a classical barrier higher than that of the preferred path by only 0.28 kcal/mol, which is similar to what was found in the previous study. However, the transition state T19 of the double-bridge-to-center process has an additional imaginary frequency mode which leads to the saddle point S7 of the preferred path.

4.4. Comparison to Recent Work. The results from the present EDIM PEF for H_2 on the Ni(100), -(110), and -(111) surfaces are consistent with those from the effective medium (EM) potential which was recently developed by Nørskov.[40] The present EDIM PEF is also theoretically similar to the EM potential in the treatment of metallic bonding. An important difference is that we used the diatomics-in-molecules (DIM) method to treat the covalent bonding interaction, whereas it is represented by the effective medium formalism plus a correction term in Nørskov's EM potential. A comparison to the earlier treatment of Lee and DePristo[41] is provided in ref 1, and the new parametrization does not change that discussion.

5. Dynamical Results

We have applied canonical variational transition state theory (CVT) with semiclassical tunneling methods to calculate the

(39) Russell, J. N., Jr.; Gates, S. M.; Yates, J. T., Jr. *J. Chem. Phys.* **1986**, *85*, 6792.

(40) Nørskov, J. K. *J. Chem. Phys.* **1989**, *90*, 7461.

(41) Lee, C. Y.; DePristo, A. E. *J. Chem. Phys.* **1986**, *84*, 485; *Ibid.* **1986**, *85*, 4161. See also ref 9.

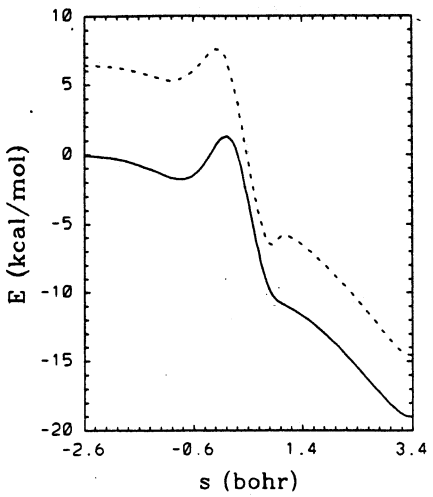

Figure 7. Plot of potential energy curves versus reaction coordinate for the lowest energy dissociative chemisorption of H_2 on Ni(100) (the bridge-to-center process). The solid line is the energy along the minimum energy path (MEP), and the dashed line is the vibrationally adiabatic ground-state potential energy curve, $V_a^G(s)$. The following critical points of Figure 1 are included: $s = -2.6$ a_0 approximates the structure R1, $s = -0.8$ a_0 corresponds to P1, $s = 0$ corresponds to S1, and $s = 3.4$ a_0 corresponds to C1.

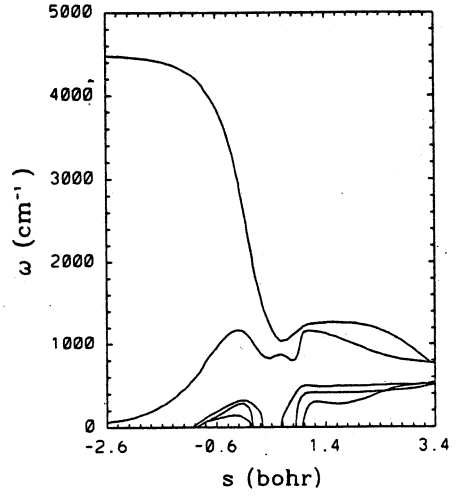

Figure 8. Plot of generalized vibrational frequencies versus reaction coordinate for the bridge-to-center dissociative chemisorption of H_2(a) on Ni(100) surface. The following critical points are included: $s = -2.6$ a_0 approximates the structure R1, $s = -0.8$ a_0 corresponds to P1, $s = 0$ corresponds to S1, and $s = 3.4$ a_0 corresponds to C1. The top line is the frequency which starts as the hydrogen stretching frequency at the reactant asymptote and is converted to one of the doubly degenerate out-of-plane frequency modes of two hydrogen atoms on the surface. The four lower frequency curves are restricted rotational and translational modes which approach zero at the reactant asymptote. In the product limit, one of these four modes is converted to the other component of the doubly degenerate out-of-plane motion, and others become the bound in-plane modes of two hydrogen atoms on the surface. The three lowest frequency modes are imaginary between roughly 0 and 1 a_0.

dissociative chemisorption rate constants of gas-phase hydrogen or deuterium molecules on Ni(100) surfaces for temperatures in the range 80–2000 K in three cases. In the first case, a clean, single face is used to model the (100) surface. For the second case, a single-layer step along the [$\bar{1}$00] direction is created on the Ni(100) surface, as described in the Computational Details section. Finally, in the third case, a partially covered surface is modeled by preadsorbing a single hydrogen atom at a stable 4-fold (center) site. In all cases, the metal surface is assumed to be rigid. Furthermore, in each case, we assume that the major contribution to the dissociation rate is from the lowest-energy dissociation path, and contributions from other higher energy dissociation paths are neglected. Other computational details are discussed in section 3.2.

5.1. H_2 and D_2 Chemisorption on Clean Ni(100). As illustrated in section 4.1, the bridge-to-center pathway is the lowest-energy route for dissociation of H_2 on the Ni(100) surface. In Figure 7, we show the classical potential energy, $V_{MEP}(s)$, and the vibrationally adiabatic potential energy, $V_a^G(s)$, along the minimum energy path for this process. Note that the maximum of the $V_a^G(s)$ curve occurs 0.16 a_0 earlier than the maximum of the $V_{MEP}(s)$ curve, which is at $s = 0$ by definition. This result indicates that the variational effect, i.e., the difference between $k^{CVT}(T)$ and $k^*(T)$, may be large, and the quantitative analysis of this effect is given below. The $V_{MEP}(s)$ curve has a little shoulder on the product side at $s \simeq 0.8$ a_0 that results in a small bump in $V_a^G(s)$ at about −6 kcal/mol; this feature is quite far into the product channel, and therefore it does not affect the CVT calculation of the dissociative chemisorption rate. Figure 7 also shows the precursor state P1 in the physisorption region near $s = -0.8$ a_0. The zero-point-energy-corrected potential energy [which is the minimum value of $\Delta V_a^G(s)$ plus the local zero-point energy along the reaction coordinate at the minimum] at this precursor state is −1.01 kcal/mol relative to the value of $V_a^G(s)$ at the reactant which is just the zero-point energy of gas-phase H_2 molecule. Thus, the effective barrier to chemisorption from the precursor state P1 is 2.22 kcal/mol (the maximum of the $V_a^G(s)$ curve relative to the zero-point-energy-corrected potential of the P1 precursor state). Because the passage over a barrier this high will be slow, it is reasonable to assume equilibrium between gas-phase H_2 and its precursor state P1 on the Ni(100) surface. The validity of this assumption has been discussed in our previous study.[9]

The generalized vibrational frequencies are plotted versus the reaction coordinates in Figure 8. These frequencies are calculated from the force constant matrix from which the direction along the reaction path has been projected out.[18-23] In general the vibrational frequencies for the EDIM bridge-to-center dissociation of H_2 on Ni(100) are quite similar to those calculated from Lee and DePristo's PEF[41] and to those calculated with the parameters of our previous study.[9] These similarities are very encouraging, the first since EDIM and Lee and DePristo's formalism are quite different and the second since it means the frequencies are not too sensitive to the changes we made here so that the parametrization is more widely useful.

Figure 8 shows that the H–H stretching frequency decreases rapidly as H_2 approaches the Ni(100) surface; at the saddle point S1 ($s = 0$), it is already lowered to only about half of its original value, although the H–H bond length is stretched by only 21%. At the chemisorption product C1, the H–H stretching mode has transformed into one of the doubly degenerate out-of-plane (z direction) frequencies of two nearly independent chemisorbed H atoms.

The other modes as s approaches $-\infty$ are hindered translational and rotational frequencies. Their frequencies increase slowly from zero as H_2 approaches the Ni(100) surface, and eventually these modes transform into the other doubly degenerate out-of-plane (z direction) and in-plane (x, y directions) frequencies of two chemisorbed H atoms. As discussed in our previous paper,[1] if one uses the bond stretching frequency in determining whether a bond is broken on a surface, one might find that this occurs at quite different bond distances when comparing various faces or even when comparing various specific sites upon which the bond dissociates.

The rate constants for the dissociative chemisorption of gas-phase H_2 and D_2 on the rigid Ni(100) surface are given in Table III for the temperature range from 80 to 2000 K. First, we consider the variational effect due to recrossing of the saddle point by trajectories located on the product side of the variational transition states, which are located at $s = -0.16$ to -0.19 a_0, depending on the temperature. This effect accounts for the CVT rate constants being lower than the conventional TST rate constants. In the present study, we found that the variational effect is large and increases rapidly as the temperature decreases in both the H_2/Ni(100) system and the D_2/Ni(100) system. The variational effect is due primarily to the s dependence of the diatom

TABLE III: Dissociative Chemisorption Rate Constants (cm^3 $molecule^{-1}$ s^{-1}) for H_2 and D_2 on the Clean Ni(100) Surface

	H_2/Ni(100)				D_2/Ni(100)			
T, K	TST	CVT	CVT/MEPSAG	CVT/SCSAG	TST	CVT	CVT/MEPSAG	CVT/SCSAG
80	3.32 (−13)[a]	2.67 (−15)	4.02 (−13)	5.23 (−13)	1.62 (−14)	9.04 (−16)	4.83 (−14)	6.54 (−14)
100	5.18 (−13)	9.48 (−15)	3.55 (−13)	4.51 (−13)	3.69 (−14)	3.12 (−15)	4.95 (−14)	6.45 (−14)
150	9.63 (−13)	5.04 (−14)	3.40 (−13)	4.07 (−13)	1.19 (−13)	1.70 (−14)	6.55 (−14)	7.83 (−14)
200	1.39 (−12)	1.20 (−13)	3.83 (−13)	4.38 (−13)	2.34 (−13)	4.25 (−14)	9.28 (−14)	1.05 (−13)
250	1.81 (−12)	2.09 (−13)	4.54 (−13)	5.02 (−13)	3.74 (−13)	7.80 (−14)	1.29 (−13)	1.41 (−13)
300	2.26 (−12)	3.14 (−13)	5.45 (−13)	5.89 (−13)	5.40 (−13)	1.23 (−13)	1.73 (−13)	1.85 (−13)
350	2.73 (−12)	4.32 (−13)	6.52 (−13)	6.93 (−13)	7.32 (−13)	1.76 (−13)	2.26 (−13)	2.37 (−13)
400	3.24 (−12)	5.63 (−13)	7.74 (−13)	8.13 (−13)	9.51 (−13)	2.38 (−13)	2.87 (−13)	2.98 (−13)
500	4.38 (−12)	8.65 (−13)	1.06 (−12)	1.10 (−12)	1.48 (−12)	3.90 (−13)	4.37 (−13)	4.48 (−13)
600	5.71 (−12)	1.22 (−12)	1.41 (−12)	1.44 (−12)	2.15 (−12)	5.82 (−13)	6.25 (−13)	6.36 (−13)
800	9.08 (−12)	2.13 (−12)	2.30 (−12)	2.34 (−12)	4.01 (−12)	1.10 (−12)	1.14 (−12)	1.15 (−12)
1000	1.36 (−11)	3.32 (−12)	3.49 (−12)	3.52 (−12)	6.69 (−12)	1.84 (−12)	1.86 (−12)	1.88 (−12)
1500	3.11 (−11)	7.89 (−12)	8.05 (−12)	8.08 (−12)	1.80 (−11)	4.84 (−12)	4.81 (−12)	4.83 (−12)
2000	5.99 (−11)	1.52 (−11)	1.54 (−11)	1.54 (−11)	3.73 (−11)	9.84 (−12)	9.73 (−12)	9.74 (−12)

[a] Power of 10 in parentheses; i.e., 3.32(−13) = 3.32×10^{-13}.

frequency, i.e., to the s dependence of the H_2 zero point requirement, and so the effect is larger for H_2 than for D_2, and this is true for all temperatures considered. In particular, the ratio of TST to CVT rate constants, k^{TST}/k^{CVT}, increases monotonically from 3.9 to 120 for the H_2/Ni(100) system, and from 3.8 to 18 for the D_2/Ni(100) system, as the temperature decreases from 2000 to 80 K.

The large barrier recrossing effect is also found in quantal mechanical studies by Jackson and Metiu[42] for H_2 dissociation on a rigid linear chain where H_2 is restricted to dissociate horizontally over an atop site (i.e., a two-degree-of-freedom system).

Table III shows also that quantum mechanical tunneling greatly enhances the dissociative chemisorption rate at low temperatures, where $k^{CVT/SCSAG}$ exceeds k^{CVT} by as much as a factor of 200. Examining the tunnel effect in more detail, we find that restricting the system to tunnel only along the MEP, that is, neglecting the reaction path curvature effect as in the CVT/MEPSAG results, the rate constant is enhanced by a factor of 1.7 at 300 K and 150 at 80 K for H_2 on Ni(100) and a factor of 1.4 at 300 K and 53 at 80 K for D_2 on Ni(100). The ratio of H_2 to D_2 tunneling enhancements increases from 1.2 at 300 K to 2.8 at 80 K in this approximation.

Including the reaction path curvature using the small-curvature approximation (SCSAG) further enhances the tunneling rate, by allowing for "corner cutting", which results in shorter tunneling paths with larger transmission probabilities.[43] As shown in Table III, the reaction path curvature effect in the CVT/SCSAG calculation further enhances the tunneling rate over the CVT/MEPSAG calculation by a factor of 1.30 for H_2 on Ni(100) and a factor of 1.35 for D_2 on Ni(100) at 80 K. This indicates, somewhat surprisingly, that "corner cutting" is more important for D_2 than for H_2 in this chemisorption reaction, although overall the H_2 dissociation has more tunneling. In fact, overall the tunneling effect increases the dissociative rate constant by a factor of 1.9 at 300 K and 200 at 80 K for H_2 on Ni(100) and by a factor of 1.5 at 300 K and 72 at 80 K for D_2 on Ni(100).

It may be useful to explain that the reason that the CVT/SCSAG rate constant for the dissociation of D_2 on Ni(100) is slightly smaller than its CVT value at 2000 K is because the transmission probability $P^G(E)$ in (19) also accounts for the nonclassical reflection contribution. Thus, at this temperature, D_2 tunneling is negligible, though nonclassical reflection reduces the CVT rate by 1%.

We also calculated the activation energies for the dissociative chemisorption of H_2 and D_2 on the Ni(100) surface by fitting the rate constants to the classical Arrhenius form

$$k(T) = Ae^{-E_a/RT} \tag{26}$$

(42) Jackson, B.; Metiu, H. *J. Chem. Phys.* **1987**, *86*, 1026.
(43) Skodje, R. T.; Truhlar, D. G.; Garrett, B. C. *J. Chem. Phys.* **1982**, *77*, 5955.

TABLE IV: Activation Energies (kcal/mol) for the Dissociation of H_2 and D_2 on Clean Ni(100)

T_1−T_2, K	$\langle T \rangle$,[a] K	H_2/Ni(100)		D_2/Ni(100)	
		CVT	CVT/SCSAG	CVT	CVT/SCSAG
80–100	89	1.01	−0.12	0.98	−0.01
100–150	120	1.00	−0.06	1.01	0.12
200–300	240	1.15	0.35	1.26	0.68
300–500	375	1.51	0.93	1.72	0.68
600–1000	750	2.98	2.66	3.44	3.22

[a] $\langle T \rangle \equiv \langle (T_1^{-1} + T_2^{-1})/2 \rangle^{-1}$.

TABLE V: Kinetic Isotope Effect for Dissociative Chemisorption of H_2 on the Clean Ni(100) Surface

T, K	TST	CVT	CVT/MEPSAG	CVT/SCSAG
80	20.47	2.96	8.33	8.00
100	14.04	3.04	7.17	6.99
150	8.08	2.97	5.19	5.19
200	5.93	2.82	4.13	4.18
250	4.84	2.68	3.52	3.57
300	4.18	2.56	3.14	3.19
350	3.74	2.46	2.88	2.92
400	3.41	2.37	2.70	2.73
500	2.96	2.22	2.43	2.45
600	2.65	2.10	2.26	2.27
800	2.26	1.93	2.02	2.03
1000	2.03	1.80	1.87	1.88
1500	1.73	1.63	1.67	1.67
2000	1.61	1.55	1.58	1.58

for several pairs of temperatures. The resulting activation energies for H_2 and D_2 on Ni(100) are given in Table IV. This procedure yields a reasonable approximation to the temperature-dependent phenomenological activation energy at the mean value of $1/T$ for each interval, and so the temperature corresponding to this mean is also tabulated. Table IV shows that the effect of quantum mechanical tunneling on the phenomenological activation energy for dissociative chemisorption of H_2 or D_2 on the Ni(100) surface is very large. This is seen by comparing the temperature dependence of the activation energies calculated from CVT and CVT/SCSAG rate constants. For both H_2 and D_2, the CVT/SCSAG activation energies decrease rapidly as the temperature decreases. In fact the calculations predict that, at 89 K, both molecules have negative activation energies for dissociative chemisorption! Since H_2 has more tunneling than the heavier D_2, the activation energies for the dissociative chemisorption of H_2 are somewhat smaller than those for D_2. At 240 K, for example, the H_2 dissociative chemisorption activation energy is 0.35 kcal/mol as compared to 0.68 kcal/mol for the H_2 dissociation, a difference 3 times larger than when tunneling is neglected.

Finally, we consider the kinetic isotope effect of the dissociative chemisorption of H_2 on the clean Ni(100) surface by examining the ratios of the H_2 to D_2 dissociation rate constants; these ratios

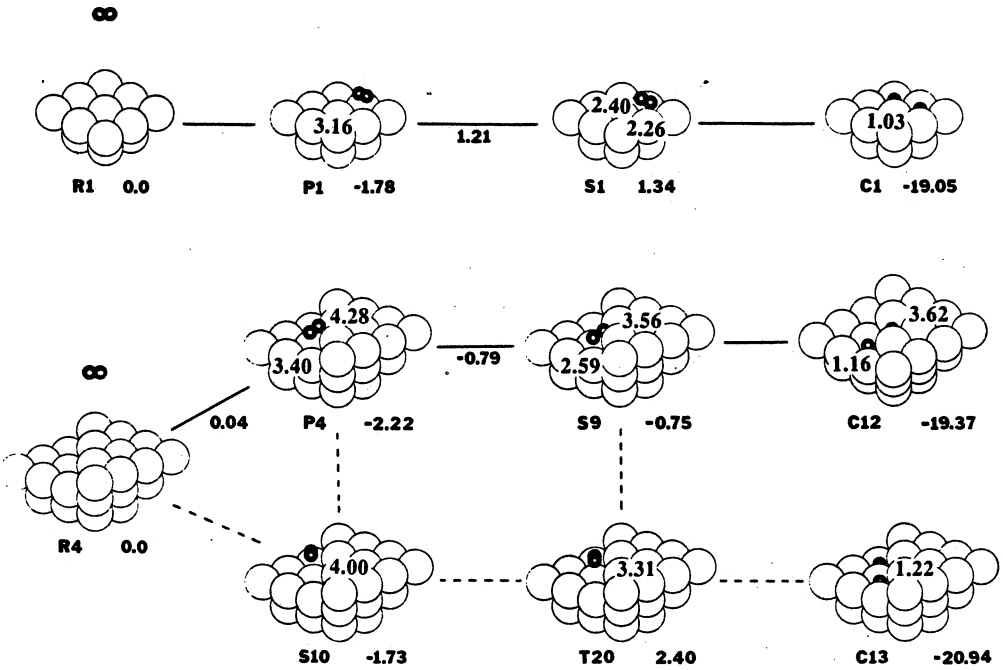

Figure 9. Same as Figure 4, except for H_2 dissociating on a [$\bar{1}$00] step of Ni(100) surface, as compared to H_2 dissociating on a terrace, as shown at the top. From the top row down are the bridge-to-center process for H_2 on the (100) terrace, the over-step process, and long-edge process at the step, respectively.

are given in Table V. Conventional TST predicts a much larger KIE than the CVT does. This results mainly from the large difference in the zero-point energies of H_2 and D_2 on Ni(100) at the chemisorption saddle point ($\Delta V_a^{\ddagger G}$ is 0.49 kcal/mol for H_2 and 0.74 kcal/mol for D_2), whereas the difference is much smaller at the respective maxima of the vibrationally adiabatic ground-state potential curves (ΔV_a^{AG} is 1.21 kcal/mol for H_2 and 1.13 kcal/mol for D_2).

Quantum mechanical tunneling, as discussed above, increases the kinetic isotope effect. Table V shows that both the CVT/MEPSAG and the CVT/SCSAG calculations predict that the ratio of H_2 to D_2 dissociation rate constants is monotonically increasing from 1.6 to 8 as the temperature decreases from 2000 to 80 K. Table IV shows that, in the low-temperature limit, the CVT/SCSAG ratio is slightly smaller than the CVT/MEPSAG one. This is due to the phenomenon discussed above that corner-cutting tunneling is more important for D_2 than H_2.

It is particularly encouraging to notice that our present theoretical prediction of the large quantum mechanical tunneling effect in the dissociative chemisorption of H_2 and D_2 on Ni(100) confirms the tunneling mechanism suggested by Hamza and Madix[12] in explaining the sticking probabilities of H_2 and D_2 on Ni(100) at low kinetic energies in their molecular beam experiment. Furthermore, the larger recrossing effect for H_2 than D_2 predicted in the present study is also consistent with the observations of Hamza and Madix.[12]

5.2. H_2 and D_2 Chemisorption at a Step on Ni(100). In this section we discuss both the statics and the dynamics of the dissociative chemisorption of H_2 and D_2 on a [$\bar{1}$00] step of the Ni(100) surface. We found that H_2 can dissociate over the step with H_2 oriented perpendicular to the direction of the step, as in the middle row of Figure 9, or along the edge of the step, as shown in the last row of Figure 9, and we refer to these processes as the over-step or along-edge processes, respectively. In the top row of Figure 9, we show the preferred bridge-to-center process for the dissociation of H_2 on the Ni(100) terrace for easy comparison. To specify geometries, we set the z coordinates of Ni atoms in the topmost full layer of Ni to be zero. With this convention the z coordinates of the Ni atoms in the half layer added to form the step are 3.326 a_0.

The along-edge dissociation proceeds through the physisorbed-like state, S10, with a classical equilibrium binding energy of 1.73 kcal/mol, and across the transition state T20 to the chemisorption state C13, where two hydrogen atoms are adsorbed 1.22 a_0 above two neighboring center sites at the bottom of the step. The classical equilibrium energy of the product state is 20.94 kcal/mol below reactants. The along-edge transition state T20 has two hydrogen atoms oriented along the step and located 3.31 a_0 symmetrically above an atop site at the bottom of the step upon which H_2 will eventually dissociate. The classical barrier height for the along-edge dissociation is 2.40 kcal/mol, which is lowered to 2.10 kcal/mol if the zero-point-energy correction at the conventional transition state is included. Note that the physisorbed state S10 and the transition state T20 are a saddle point and a higher order transition state, respectively, and following one of the imaginary frequency modes in each case leads to the corresponding precursor state and saddle point of the over-step dissociation. The over-step process is the preferred route for dissociation at the step. The saddle point along this route has a classical barrier height 0.75 kcal/mol below the zero of energy where H_2 is infinitely far from the surface, and the associated vibrationally adiabatic ground-state barrier which occurs between P4 and S9 is 0.79 kcal/mol below the total internal energy of the reactant (zero-point energy of H_2 stretching mode). Thus the rate limiting effective barrier for the dissociation of H_2 over the step of the Ni(100) surface occurs prior to the precursor state. Figure 10 shows that the V_{MEP} curve has a flat local minimum associated with the precursor P4, with a classical equilibrium binding energy of 2.22 kcal/mol. Notice that the precursor state P4 is 0.44 kcal/mol more stable than the precursor state S1 for H_2 on the clean Ni(100) terrace. Before examining the geometry of H_2 along the MEP in an attempt to understand the nature of the flat region near the precursor P4, we discuss briefly the method of choosing the optimal starting point for calculating the early part of the MEP.

First, let the step be along the y axis and the over-step dissociation proceed along the x axis. For each distance z_{cm} of the center of mass sufficiently high above the full-layer surface plane, we optimize the H_2 orientation in the xz plane and the location of H_2 along the dissociation path (the x_{cm} coordinate of the center of mass of H_2) while keeping the H_2 bond length fixed at its gas-phase equilibrium value. The optimized geometry is then used as a starting point for calculating the physisorption part of the MEP. As the distance z_{cm} increases from 6 a_0, we find that the MEP is converged in the most significant region at z_{cm} equal to 8 a_0.

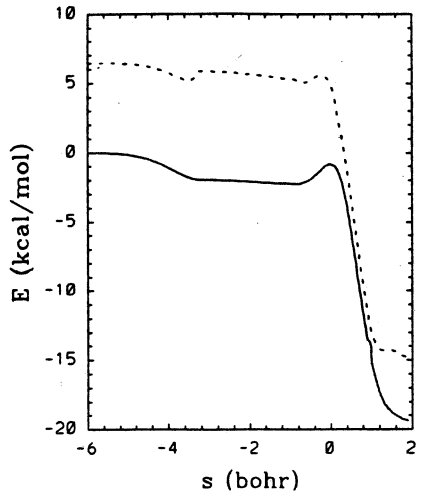

Figure 10. Same as Figure 7, except for the over-step process of H_2 at the [$\bar{1}$00] step on the (100) face. The following critical points of Figure 9 are included: $s = -6$ a_0 approximates the structure R4, $s = -0.75$ a_0 corresponds to P4, $s = 0$ corresponds to S9, and $s = 1.95$ a_0 corresponds to C12.

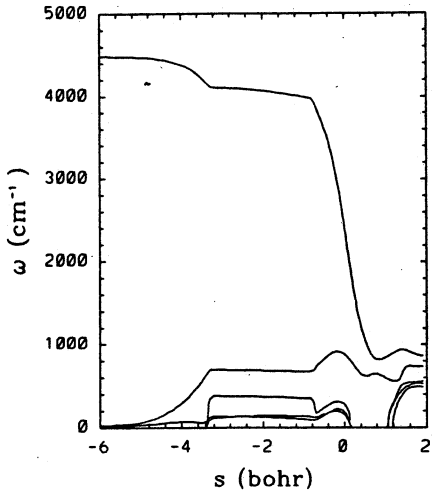

Figure 11. Same as Figure 8, except for the over-step dissociation process. The critical points included are the same as in Figure 10.

Sufficiently high above the surface, the potential energy of interaction is dominated by the embedded energy contributions, F_i; thus it is attractive, and we find that H_2 prefers to remain close to the step as it approaches the surface while the energy decreases steadily. However, as the H_2 begins to experience significant interactions, at $s \cong -3.2$ a_0, where $z_{cm} \cong 5.47$ a_0 and $x_{cm} \cong -1.13$ a_0, the short-range repulsive interaction with the step becomes important and causes the MEP to move further out from the step until reaching the precursor state at $s = -0.76$ a_0, where $z_{cm} = 3.89$ a_0 and $x_{cm} = -2.95$ a_0. The competition between the embedded F_i and repulsive ϕ_{ij} interactions results in the flat region between $s = -3.2$ a_0 and -0.76 a_0 on the V_{MEP}.

There is a remarkable similarity in the saddle point structures of the over-step dissociation process discussed here and the preferred center-to-long-bridge dissociation of H_2 on Ni(110) as discussed in section 4.2. First, from the surface-structure standpoint, the regions of the two adsorption sites of the chemisorption product C12, i.e., the region of the center site at the bottom of the step and at the opened-center (missing one Ni atom to form a regular 4-fold) site at the top of the step, are spatially similar to the valley of the Ni(110) surface. As a consequence, H_2 is able to approach much closer to the metal surface, thus gaining substantial attractive gas–metal interaction energy which can compensate or even exceed the energy required by the system to stretch the H–H bond at the chemisorption transition state and the repulsive interaction, and this results in the absence of a barrier to chemisorption for the over-step process. In particular, at the saddle point S9 of the over-step process (Figure 9), the hydrogen atom that is closer to the top of the step is only 0.23 a_0 above the top surface plane, and the H–H bond length is stretched by only 17%. In comparison, at the saddle point structure S2 of the center-to-long-bridge dissociation of H_2 on Ni(110) (Figure 5), the H–H bond length is also stretched by only 15%. The vibrational frequencies at these two saddle points S2 and S9 are quite similar as well; for instance the imaginary frequencies are $808i$ and $727i$ cm^{-1} and the H–H stretch frequencies are 2467 and 2447 cm^{-1} for S2 and S9, respectively.

The vibrational frequencies along the MEP of the over-step process are shown in Figure 11; they have similar features to the frequencies for bridge-to-center dissociation of H_2 on Ni(100) as shown in Figure 8, except that, for the over-step process, the frequencies change by a negligible amount over the flat region of the precursor state P4. As mentioned earlier, at the saddle point S9, the H–H stretching frequency is 2447 cm^{-1}, which is 45% lower than for gas-phase H_2 infinitely far from the surface.

The calculated rate constants for the dissociative chemisorption of H_2 and D_2 at the step are given in Table VI. Note that the final (CVT/CAG) rate constants for H_2 and D_2 dissociative chemisorption at a step are consistently larger than the final (CVT/SCSAG) rate constants for dissociation over a terrace (as given in Table III). The difference for H_2 ranges from a factor of 1.4 at the high-temperature limit to nearly an order of magnitude at the low-temperature limit. The differences for D_2 are slightly larger.

TABLE VI: Rate Constants (cm^3 $molecule^{-1}$ s^{-1}) and Kinetic Isotope Effects for H_2 and D_2 Dissociative Chemisorption at a [$\bar{1}$00] Step on the (100) Surface

	CVT/CAG		
T, K	H_2	D_2	KIE
80	4.67 (−12)[a]	8.44 (−13)	5.54
100	4.07 (−12)	7.12 (−13)	5.71
150	3.44 (−12)	5.97 (−13)	5.77
200	3.26 (−12)	5.91 (−13)	5.51
250	1.98 (−12)	6.28 (−13)	3.16
300	2.02 (−12)	6.89 (−13)	2.93
350	2.12 (−12)	7.69 (−13)	2.75
400	2.26 (−12)	8.65 (−13)	2.61
500	2.63 (−12)	1.10 (−12)	2.39
600	3.10 (−12)	1.39 (−12)	2.23
800	4.35 (−12)	2.17 (−12)	2.00
1000	5.99 (−12)	3.22 (−12)	1.86
1500	1.21 (−11)	7.30 (−12)	1.66
2000	2.17 (−11)	1.38 (−11)	1.57

[a] Power of 10 in parentheses; i.e., 4.67 (−12) = 4.67×10^{-12}.

TABLE VII: Activation Energies (kcal/mol) Calculated by the CVT/CAG Method for the Dissociation of H_2 and D_2 at a Step on Ni(100)

T_1–T_2, K	$\langle T \rangle$,[a] K	H_2	D_2
80–100	89	−0.11	−0.14
100–150	120	−0.10	−0.11
200–300	240	−0.57	0.18
300–500	375	0.39	0.70
600–1000	750	1.96	2.50

[a] $\langle T \rangle \equiv \langle (T_1^{-1} + T_2^{-1})/2 \rangle^{-1}$.

The activation energies calculated from the Arrhenius equation, (25), for different pairs of tempreatures are given in Table VII. The results show that, for temperatures below 300 K, the dissociation of H_2 on the step of the Ni(100) surface has a negative activation energy, and a similar result is obtained for D_2 at temperatures below 150 K. At higher temperatures, both dissociations of H_2 and D_2 on the step of Ni(100) have positive activation energies, although they are smaller than the corresponding values of H_2 and D_2 dissociating on the clean Ni(100) surface.

Finally, we consider the kinetic isotope effect (KIE) for the dissociation of H_2 on the [$\bar{1}$00] step of Ni(100). The ratios of H_2 CVT/CAG rate constants to D_2 ones are also given in Table

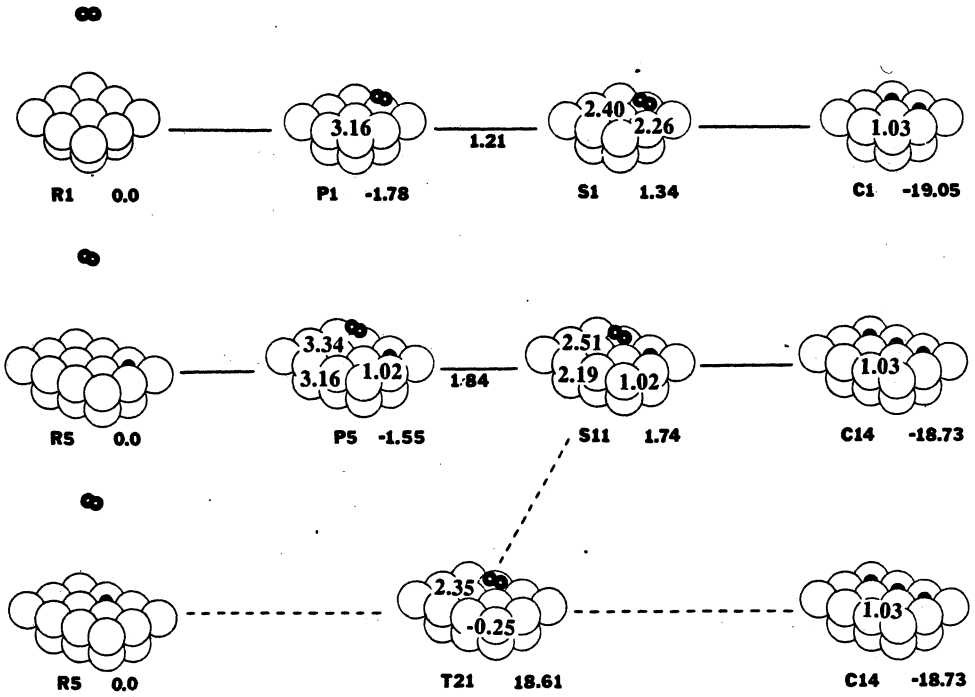

Figure 12. Same as Figure 4, except for H_2 dissociating on the partially covered (100) surface. (The top row compares this to H_2 dissociating on a clean surface.) From the top down are the bridge-to-center process of H_2 on the clean Ni(100) surface, the aside bridge-to-center process on the partially covered surface, and the on-top center-to-center process on the partially covered surface, respectively.

VI. We see that the KIE monotonically increases from 1.6 to 5.8 as the temperature is decreased from 2000 to 150 K. Although the magnitude of the KIE is rather large, it is smaller than the KIE for dissociation on a terrace, except for the temperature interval of 150–200 K. However, for temperatures above room temperature, the difference in the KIE for H_2 dissociating on the stepped surface and the terrace is small.

Although we have only presented detailed results for reaction at a step, it should be clear that dynamics at more complicated surface features, such as kinks, could also be studied with the present parametrization.

It is interesting to point out that the present results of a higher binding energy at the precursor state and a lower barrier for H_2 dissociating over the step, compared to those for H_2 dissociating on a clean Ni(100) terrace, support the argument of Zhu et al.[38] for the appearance of the precursor-mediated dynamics; that is, at low temperatures, H_2 molecules that do not have sufficient energy to overcome the barrier to chemisorption on the terrace may move to surface defects such as steps and dissociate. The present results are also consistent with experimental observations by Mårtensson et al.,[44] where a molecular adsorbed H_2 state at a step is detected but no such state is observed on the flat terrace. However, the binding site at a step for H_2 at low coverage as predicted in the present study is different from what has been suggested by Mårtensson et al.[44] for H_2 on the covered step surface.

5.3. H_2 and D_2 Chemisorption on Partially Covered Ni(100). In this section, we consider the statics and dynamics of the dissociation of H_2 and D_2 on a partially covered Ni(100) surface. The partially covered Ni(100) surface is modeled by adsorbing one H atom at a center site, and we consider the situation where the adatom effect is maximized by restricting attention to the cases where H_2 dissociates either on the top of the adatom or at the nearest empty sites, as shown in the last and middle rows of Figure 12, respectively. We refer to these two cases as the on-top center-to-center and aside bridge-to-center processes. In the top row of Figure 12 we show the preferred bridge-to-center dissociation of H_2 on the clean Ni(100) surface for easy comparison. Two-dimensional energy contour plots for the on-top center-to-center and aside bridge-to-center processes are shown in Figure 13a and 13b, respectively. These contour plots are similar to Figures 1–3, except that the geometry of the adsorbed H atom is optimized at every grid point.

As shown in Figures 12 and 13a, the on-top center-to-center dissociation of H_2 is a direct process with a large classical barrier height of 18.61 kcal/mol. The large barrier for the on-top process can be appreciated immediately from the transition-state structure, T21. At this transition state, H_2 is required to get very close to the surface; as a result, it pushes the adsorbed H atom 0.25 a_0 below the surface plane into the bulk. The process illustrated in the middle row appears to be the lowest energy process in which H_2 dissociates either on the top of the adatom or at one of the nearest empty sites. The aside bridge-to-center process proceeds through the precursor state P5, crosses the saddle point S11, and finally forms the chemisorption produce C14. The geometry of H_2 along this path is somewhat similar to that of the bridge-to-center dissociation of H_2 on the clean Ni(100) surface. The small differences are due to the presence of the adsorbed H atom; for instance, at the stationary points P5 and S11, the H_2 molecule is pushed closer to the remote bridge site upon which it dissociates. As a result of these adsorbate–adsorbate repulsive interactions, the classical equilibrium binding energy of the precursor state P5 is 1.55 kcal/mol, which is 0.23 kcal/mol less than for the corresponding P1 state, and the classical barrier to dissociation is 1.74 kcal/mol, which is 0.37 kcal/mol higher than that of H_2 dissociating on the clean surface. The effect on the vibrationally adiabatic ground-state barrier heights, ΔV_a^{AG}, is more significant; in particular the presence of an adsorbed H atom raises ΔV_a^{AG} for the preferred bridge-to-center dissociation of H_2 on Ni(100) by 0.63 kcal/mol. Thus the adsorbed H atom acts as a poison (rather than a cocatalyst) to the dissociative chemisorption process.

We have calculated the rate constants for the aside bridge-to-center process by CVT/SCSAG theory. The results could be used in a kinetic model of the dynamics of the dissociative chemisorption of H_2 on a partially covered surface by assigning different rates to dissociation near and far from previously covered sites.

The rate constants for the aside bridge-to-center dissociation are given in Table VIII for the temperature range from 80 to 2000 K. First, notice that the variational (recrossing) effects for both H_2 and D_2 dissociation on the covered surface are generally smaller

(44) Martensson, A.-S.; Nyberg, C.; Andersson, S. *Phys. Rev. Lett.* **1986**, *57*, 2045.

TABLE VIII: Dissociative Chemisorption Rate Constants (cm^3 $molecule^{-1}$ s^{-1}) for H_2 and D_2 on the Partially Covered H/Ni(100) Surface

	H_2 + H/Ni(100)				D_2 + D/Ni(100)			
T, K	TST	CVT	CVT/MEPSAG	CVT/SCSAG	TST	CVT	CVT/MEPSAG	CVT/SCSAG
80	2.43 (-15)[a]	4.78 (-17)	7.63 (-14)	1.28 (-13)	1.84 (-16)	2.09 (-17)	5.57 (-15)	9.22 (-15)
100	8.57 (-15)	3.60 (-16)	6.86 (-14)	1.11 (-13)	8.45 (-16)	1.42 (-16)	6.09 (-15)	1.01 (-14)
150	4.53 (-14)	5.08 (-15)	7.21 (-14)	1.05 (-13)	6.76 (-15)	1.86 (-15)	1.03 (-14)	1.44 (-14)
200	1.08 (-13)	1.93 (-14)	9.21 (-14)	1.22 (-13)	2.06 (-14)	7.15 (-15)	1.85 (-14)	2.30 (-14)
250	1.89 (-13)	4.43 (-14)	1.23 (-13)	1.52 (-13)	4.28 (-14)	1.69 (-14)	3.08 (-14)	3.58 (-14)
300	2.84 (-13)	7.95 (-14)	1.62 (-13)	1.91 (-13)	7.33 (-14)	3.14 (-14)	4.75 (-14)	5.29 (-14)
350	3.93 (-13)	1.24 (-13)	2.10 (-13)	2.38 (-13)	1.12 (-13)	5.08 (-14)	6.86 (-14)	7.43 (-14)
400	5.15 (-13)	1.78 (-13)	2.66 (-13)	2.94 (-13)	1.59 (-13)	7.52 (-14)	9.44 (-14)	1.00 (-13)
500	8.00 (-13)	3.10 (-13)	4.03 (-13)	4.30 (-13)	2.82 (-13)	1.40 (-13)	1.61 (-13)	1.67 (-13)
600	1.14 (-12)	4.78 (-13)	5.72 (-13)	6.00 (-13)	4.44 (-13)	2.26 (-13)	2.49 (-13)	2.56 (-13)
800	2.03 (-12)	9.23 (-13)	1.02 (-12)	1.05 (-12)	9.15 (-13)	4.77 (-13)	5.01 (-13)	5.09 (-13)
1000	3.24 (-12)	1.54 (-12)	1.64 (-12)	1.67 (-12)	1.62 (-12)	8.47 (-13)	8.71 (-13)	8.80 (-13)
1500	8.08 (-12)	3.96 (-12)	4.08 (-12)	4.11 (-12)	4.70 (-12)	2.43 (-12)	2.44 (-12)	2.45 (-12)
2000	1.62 (-11)	7.97 (-12)	8.09 (-12)	8.13 (-12)	1.01 (-11)	5.15 (-12)	5.14 (-12)	5.15 (-12)

[a] Power of 10 in parentheses; i.e., 2.43 (-15) = 2.43×10^{-15}.

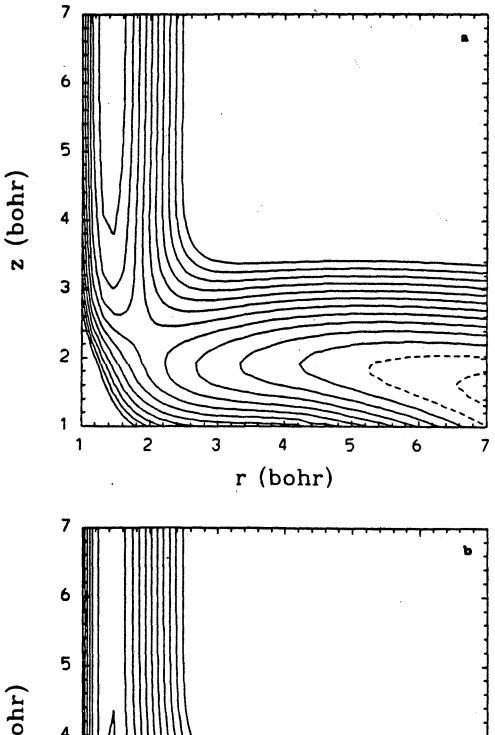

Figure 13. (a) Same as Figure 1, except for the on-top center-to-center dissociation of H_2 on the partially covered Ni(100) surface with the center of mass and orientation of H_2 corresponding to structures T21 and C14. Contour levels are from −10 to 50 kcal/mol. (b) Same, except for the aside bridge-to-center process, with the center of mass and orientation of H_2 corresponding to structure C14.

than those for the clean surface. In addition, the presence of the adsorbed H atom near the dissociating site substantially enhances the relative importance of the tunneling mechanism for dissociation, especially at low temperatures. Nevertheless, the final CVT/SCSAG rate constants for both H_2 and D_2 on the covered surface are smaller than those obtained from dissociating on the clean surface. These results are consistent with the experimental

TABLE IX: Kinetic Isotope Effect for Dissociative Chemisorption of H_2 and D_2 on the Partially Covered Ni(100) Surface

T, K	TST	CVT	CVT/MEPSAG	CVT/SCSAG
80	13.20	2.28	13.70	12.94
100	10.14	2.54	11.27	10.98
150	6.70	2.73	7.02	7.30
200	5.22	2.70	4.98	5.30
250	4.41	2.62	3.98	4.23
300	3.88	2.53	3.42	3.61
350	3.51	2.44	3.07	3.20
400	3.23	2.36	2.82	2.93
500	2.84	2.23	2.50	2.57
600	2.57	2.11	2.30	2.34
800	2.22	1.94	2.04	2.06
1000	2.00	1.81	1.88	1.90
1500	1.72	1.63	1.67	1.68
2000	1.60	1.55	1.58	1.58

observation of Hamza and Madix[12] that the initial sticking probability of H_2 decreases with increasing coverage. The ratios of H_2 to D_2 dissociative chemisorption rate constants for dissociation next to an occupied site are given in Table IX. The table shows that the KIE is larger than for dissociation on the clean surface, especially at low temperatures. Thus we predict a KIE that increases with increasing surface coverage. The increase of the KIE is most directly attributable to the enhancement in the tunneling rate by a nearby adsorbed H atom; the enhancement factor is larger for the lighter molecule H_2 than for the heavier D_2.

6. H + H_2 Exchange Reaction on Ni(100)

As discussed in section 2.2, the present EDIM parameter set allows us not only to treat H and H_2 interactions with a metal surface but also to treat H + H_2 reactions at the surface. In particular the parameters are able to reproduce the accurate gas-phase H + H_2 exchange barrier. Thus, it is possible, in the present study, to investigate the possibility of direct exchange reaction H + H_2 on a metal surface such as Ni(100) in this case. This is a prototype for catalysis of a covalent exchange reaction in general. For the convenience of the following discussion, we labeled the H atoms; thus we investigate the reaction

$$H_a/Ni(100) + H_bH_c/Ni(100) \rightarrow H_aH_b/Ni(100) + H_c/Ni(100) \quad (27)$$

where H_b is the atom being exchanged.

From the topology of the Ni(100) surface, there are two possibilities for a direct exchange reaction to occur in a plane parallel to the crystal face. In one case the H_a–H_b–H_c bond angle is 180°, and in the other it is 90°; these are called the collinear and perpendicular paths. In Figures 14 and 15 we show the potential energy in the r_1–r_2 plane where r_1 is the bond distance H_a–H_b and r_2 is H_b–H_c distance. Figure 14 is for the collinear path, and

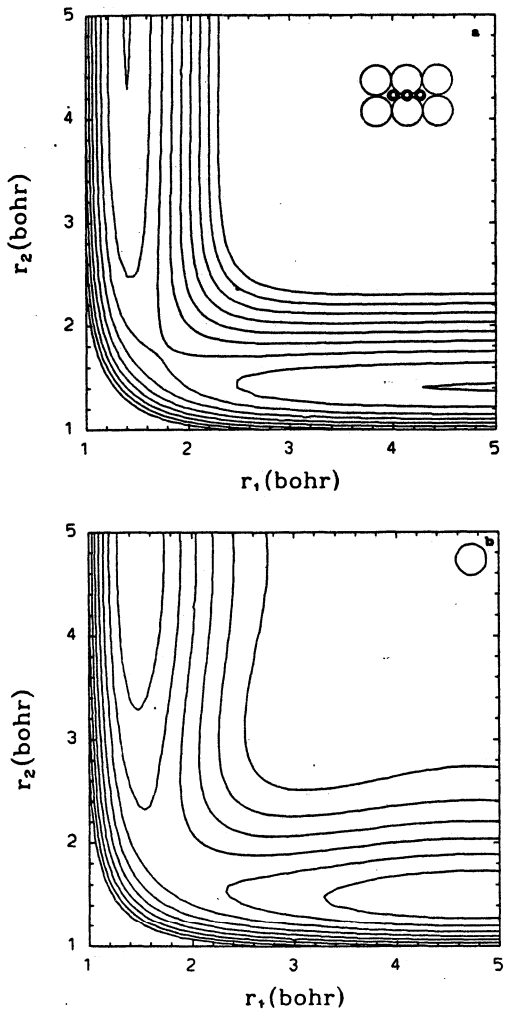

Figure 14. EDIM potential energy contours for the over-bridge collinear exchange reaction $H_a + H_bH_c \rightarrow H_aH_b + H_c$ on the Ni(100) surface plotted against the H_a–H_b bond distance, r_1 (a_0), and the H_b–H_c bond distance, r_2 (a_0). All three H atoms have a fixed z coordinate (height above the surface). The relative position of the H_3 system to the metal surface is shown in the top right corner of (a). The zero of energy is defined as the sum of the binding energies of the adsorbed H_a atom, and of the optimized H_bH_c, both at a given z coordinate. The contour interval is 5 kcal/mol. (a) $z = 5$ a_0 and the contour levels are from 0 to 40 kcal/mol. (b) $z = 3$ a_0, and the contour levels are from 0 to 30 kcal/mol.

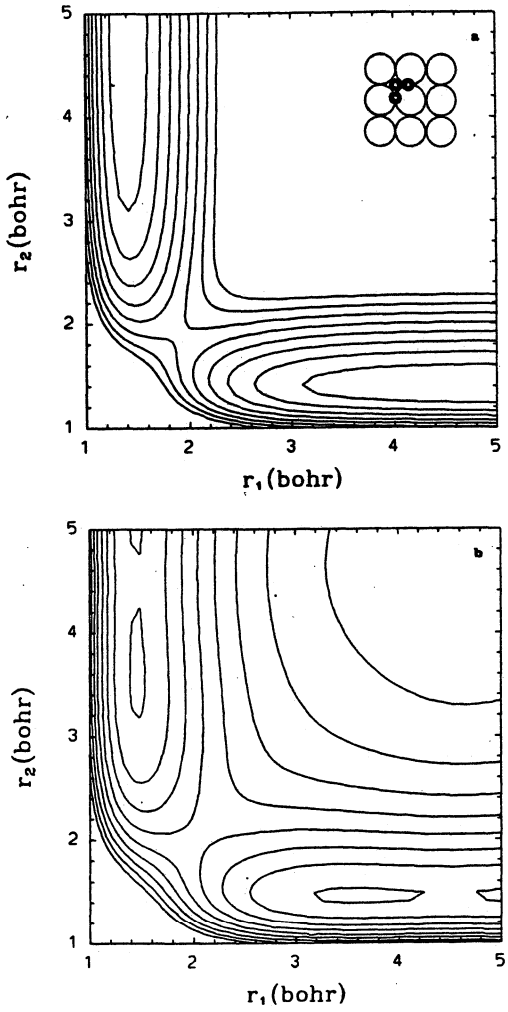

Figure 15. Same as Figure 14 except for the perpendicular exchange reaction. (a) $z = 5$ a_0 and the contour levels are from 5 to 40 kcal/mol. (b) $z = 3$ a_0 and the contour levels are from 0 to 35 kcal/mol.

Figure 15 is for the perpendicular path. In both figures, all three H atoms are at a fixed height above the surface plane (constant z coordinates); in Figures 14a and 15a this height is 5 a_0 and in Figures 14b and 15b, $z = 3$ a_0.

In Figure 14 we consider a collinear exchange reaction where the H_b atom is fixed at a bridge site, while H_a and H_c move from and to the two oppositely situated center sites. We refer to this as the over-bridge collinear process. In Figure 15, we look at the perpendicular exchange reaction where H_b is fixed at a center site, while H_a and H_c move from and to the two nearest center sites at right angle to each other. In all cases (Figures 13 and 14), the energy is relative to a reference situation in which H_a is above a center site at the given fixed z value and H_bH_c is at an optimized bond distance, again at the given fixed z coordinate.

At 5 a_0 above the surface, the contours for the collinear exchange reaction are nearly the same as in the gas phase ($z = \infty$), and the perpendicular exchange reaction has a significantly larger barrier, again similar to the situation in the gas phase. Figures 14b and 15b show that both routes have lower barriers at $z = 3$ a_0, but the colinear exchange barrier remains lower. Thus, we focused our attention on locating the real nine-dimensional saddle point for the collinear reaction. In the gas phase as well as at $z = 3$ and 5 a_0, the saddle point structure is symmetric; i.e., $r_1 = r_2$; thus the saddle point is the minimum along the equal bond

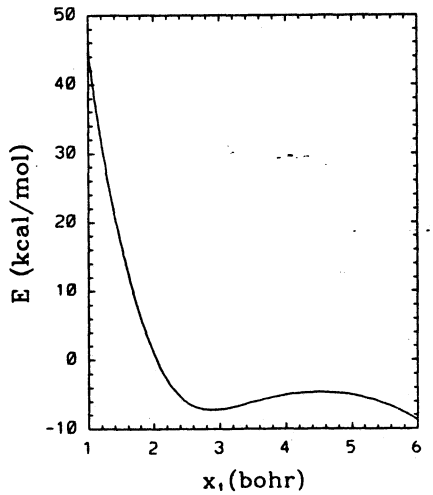

Figure 16. Plot of energy of the symmetrical $H_a\cdots H_b\cdots H_c$ system on Ni(100) for the collinear over-bridge exchange reaction where the H_a–H_b bond distance equals the H_b–H_c bond distance versus the projected H_a–H_b bond distance, x_1 (a_0). The zero of energy is defined to be the sum of the H(a) binding energy at a center site and the H_2(a) binding energy at the precursor state P1.

distance cut (the line of slope 1 in the contour plots). For the next plot, Figure 16, let the x axis be the line containing the three atoms, with H_b at the origin and also above a bridge site and H_a on the positive side of x. Thus, x_1, the x coordinate of the H_a atom, is also the bond distance r_1 projected on the x axis (x_1 =

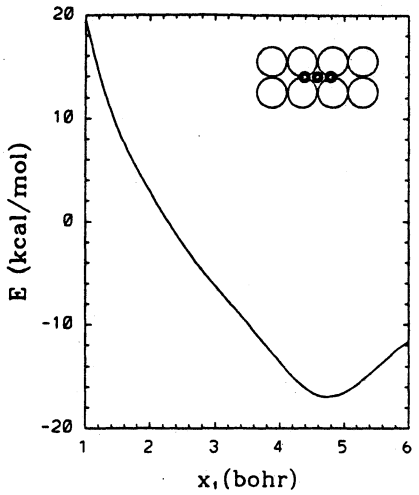

Figure 17. Same as Figure 16 except for the collinear over-center exchange reaction where the exchanged H_b atom is located above a center site of Ni(100). The position of the H_a···H_b···H_c complex relative to the surface is shown in the top right corner of the plot.

r_1 if H_aH_b is parallel to the surface). In Figure 16, we plot the energy of the H_a···H_b···H_c/Ni(100) complex versus the x_1 coordinate, where the complex has equal projected bond instances x_1 and x_2 and all z coordinates of the H atoms are optimized for each x_1. Note that the gradients in the y direction of all three H atoms are zero due to the symmetry of the reaction. Thus, the minima of the potential energy plotted against x_1 correspond to the true symmetric nine-dimensional transition state for the direct exchange reaction, if it exists, and to chemisorption states. However, as shown in Figure 16, the first local minimum occurs at x_1 about 2.7 a_0, and it corresponds to a chemisorption state, since it has all positive definite vibrational frequencies.

We also investigated the possibility that the collinear exchange reaction occurs over a center site (the exchanged H_b atom is located directly above a center site at the transition state). Similar to the over-bridge site case, the energy versus the projected bond distance shown in Figure 17 has the first local minimum, though at a much larger x_1, corresponding to a chemisorption state. In conclusion, we found there is no direct exchange reaction on the Ni(100) surface. Furthermore, the total energy of 3H(a), where the three H atoms are at equilibrium positions above three neighboring center sites, is about 86 and 54 kcal/mol below the saddle points energies of Figure 14a and 14b, respectively, with the same zero of energies as used in the plots. Recall that the barrier for the recombination and desorption of H_2 on Ni(100) is about 22 kcal/mol. Therefore, the exchange reaction on Ni(100) has a two-step mechanism, first dissociative chemisorption and then recombinative desorption. These results can be physically rationalized as follows. In the gas-phase reaction, both H and H_2 are freely moving in three-dimensional space, whereas on a metal surface, their motions are somewhat restricted due to the surface topology and depend on the magnitude of the adsorbate–substrate interactions. For the present case, the adsorbed H atom is mostly localized at about 1 a_0 above a center site, while the physisorbed H_2 molecule can move rather freely through the physisorbed corrugated well, which is about 3 a_0 above the metal surface. In order for a direct exchange reaction to occur, the adsorbed H and H_2 must be closer together at the transition state. The only way to achieve this is by pulling an adsorbed H atom up to about the same height as that of the adsorbed H_2; this would require an energy close to the H binding energy, 64 kcal/mol; thus it is very unlikely. On the other hand, the physisorbed H_2 can first dissociate, and this requires an energy of about 1 kcal/mol to surmount the barrier to chemisorption. Once dissociated, the H atom of the H_2 molecule can diffuse along the surface to recombine with the coadsorbed H atom, and the barriers for diffusion and desorption are of the order 4 and 22 kcal/mol, respectively. Thus, the two-step mechanism for the exchange reaction on Ni(100) is more favorable.

7. Conclusion

In the present study, we have presented a new parametrization for the EDIM PEF that is more generally applicable than the previous one. In particular it can be used to study reactions at steps or kinks, and it is also parametrized for systems of three H atoms on a Ni surface. In addition the new parametrization is more accurate even for two H atoms on the surface because it is based on variational transition states rather than saddle points.

We have carried out canonical variational transition state theory calculations with semiclassical ground-state transmission coefficients to calculate rate constants and kinetic isotope effects (KIEs) for the dissociative chemisorption of H_2 molecules on three types of Ni(100) surface, namely, clean terraces, clean steps, and partially covered terraces. We found that both recrossing and tunneling effects are important for the dissociative chemisorption of H_2 on the clean Ni(100) surface. The resulting activation energies and the large KIEs are consistent with experimental observations. The presence of a step on the Ni(100) surface is found to enhance the dissociative chemisorption rate significantly, while decreasing the KIE. On the other hand, if the surface is partially covered with chemisorbed H, the further dissociative chemisorption of H_2 and D_2 rate decreases, while the KIE increases, and these results are also consistent with experimental data. In the present study, we found that there is no direct H + H_2 exchange reaction on Ni(100); however, the exchange reaction on the metal surface should occur in two steps, first dissociative chemisorption and then recombinative desorption.

Acknowledgment. We are grateful to Bruce Garrett for helpful discussions. This work was supported in part by the National Science Foundation and Minnesota Supercomputer Institute.

Registry No. Ni, 7440-02-0; H_2, 1333-74-0; D_2, 7782-39-0; H, 12385-13-6.